Translesion DNA synthesis polymerase κ is essential to a carcinogen-induced nucleolar stress response

Shilpi Paul[1,2*], Abbey Rebok[1#], Paolo Cifani[3#], Anirban Paul[2#], Darryl Pappin[3], Tony T. Huang[4], Thomas E. Spratt[1*]

[1]Biochemistry and Molecular Biology, Penn State College of Medicine, Hershey, PA, USA

[2]Neural and Behavioral Sciences, Penn State College of Medicine, Hershey, PA, USA

[3]Cold Spring Harbor Laboratory, Cold Spring Harbor, NY, USA

[4]Biochemistry and Molecular Pharmacology, New York University School of Medicine, NY, USA

# equal contribution

*Corresponding author shilpi@psu.edu and tes13@psu.edu

Abstract

DNA polymerase kappa (Polκ) has multiple cellular roles such as translesion DNA synthesis, replication of repetitive sequences and nucleotide excision repair. However, the mechanisms regulating Polκ's cellular activities are unknown. Since all polymerases insert the canonical deoxynucleotide triphosphates, it is difficult to determine which polymerase is active at a particular genomic site. To counter this difficulty, we utilized the selective Polκ substrate, N^2-(4-ethynylbenyl)-2'-deoxyguanosine (EBndG), as bait to capture proteins associated with Polκ synthesized DNA. Here we show that, Polκ is active in the nucleolus and Polκ synthesized DNA are enriched with nucleolar proteins. Exposure of cells to benzo[*a*]pyrene diol epoxide

(BPDE) induced hallmarks of nucleolar stress, increased Polκ stability and nucleolar activity. Other agents that induce nucleolar stress such as mitomycin C, cisplatin and actinomycin D also increased Polκ's nucleolar activity. The Polκ activity was cell-cycle independent and dependent on PCNA ubiquitination. In addition, we identified that the expression and activity of Polκ is regulated by the polycomb complex protein Ring Finger Protein 2 (RNF2) and by poly(ADP)-ribose polymerase 1 (PARP1) catalyzed PARylation. This study provides insight into the novel role of Polκ in ribosomal RNA synthesis, in maintaining ribosomal DNA integrity after DNA damage thus protecting the cells from nucleolar stress.

Introduction

DNA polymerase κ (Polκ) is one of the sixteen DNA-dependent DNA polymerases expressed in humans [1]. The most-studied function of Polκ is translesion DNA synthesis (TLS), which is one of the mechanisms by which the cell responds to DNA damage that cannot be replicated by high fidelity DNA polymerases. The carcinogen (+/-)-*trans*-benzo[*a*]pyrene-7,8-dihydrodiol-9,10-epoxide (BPDE) covalently reacts with deoxyguanosine generating 10-(deoxyguanosin-N^2-yl)-7,8,9-trihydroxy-7,8,9,10-tetrahydrobenzo[*a*]pyrene (N^2-BP-dG) [2], which Polκ can bypass by inserting dCMP efficiently opposite such bulky N^2-alkyl-dG adducts [3–7]. Thus, Polκ plays a critical role in recovery from BPDE-induced S-phase checkpoint arrest by being recruited to the stalled replication fork facilitated by the E3 ligase Rad18 -mediated PCNA monoubiquitination [8]. While the TLS function of Polκ has been the most-studied, other functions of Polκ are being elucidated. Polκ has been linked with nucleotide excision repair [9],

cross-link repair [10,11], the production of short oligodeoxynucleotides in the ATR activation pathway [12] and in replication of repetitive DNA sequences [13,14]. A hurdle with determining when and where a specific DNA polymerase is active is that all polymerases utilize undamaged DNA and the four deoxynucleotide triphosphates as substrates. To overcome this impediment, we utilized N^2-4-ethynylbenzyl-2´-deoxyguanosine (EBndG), a non-natural nucleoside that has high specificity for Polκ over other mammalian DNA polymerases [15]. Using this tool, we identified a role for Polκ in the repair of ribosomal DNA (rDNA).

rDNA is present in the human genome in hundreds of copies. The 5.8S, 18S, and 28S rDNA sequences are located within the nucleolar organizer regions (NORs) on the short p-arms of chromosomes 13, 14, 15, 21 and 22. The rRNA is transcribed as a single transcript to form a 47S pre-rRNA that is processed in the nucleolus before being assembled as the ribosome in the cytoplasm. rDNA is the most actively transcribed regions in the genome and ribosome production comprises the bulk of the energy consumption of the cell [16].

The repetitive nature of the NORs, presence of rDNA genes in clusters on five different chromosomes, high transcription rate that creates conflicts with replication forks [16] lead to replication stress (RS) [17,18]. The transcription-associated R-loops that are formed due to negative supercoiling of DNA behind a transcription bubble and the opening of DNA strands forming stable RNA:DNA hybrids [19,20] are increased under RS [21]. Persistent RS and R-loops create replication fork slowing and stalling that can lead to long stretches of single-stranded DNA (ssDNA) and single-strand DNA breaks (SSBs). In situations that leads stalled forks to collapse, SSBs convert into double-strand breaks (DSBs) and make the rDNA genes highly vulnerable to DNA damage [22].

Active transcription of rDNA by RNA polymerase I (RNAPI) initiates nucleoli formation, a membrane-less compartment in the nucleus created by liquid-liquid phase separation. The nucleoli are dispersed during mitosis, and then small nucleoli containing individual NORs are reformed during telophase when rRNA transcription resumes. With progression of the cell cycle, nucleoli fuse and form larger nucleoli containing multiple NORs. The nucleolus is a "tripartite" nuclear structure with multiple sub-compartments, the fibrillar center (FC), the dense fibrillar component (DFC) and the granular component (GC) [23,24]. Transcription of pre-ribosomal RNA (pre-rRNA) occurs at the interface of the FC and DFC compartments. The FC is enriched in components of the RNAPI machinery, such as upstream binding transcription factor (UBF1), DFC contains pre-rRNA processing factors such as fibrillarin (FBL), and the GC, where preribosome subunit assembly occurs, contains nucleophosmin (NPM1).

The nucleolus responds to different types of DNA damaging agents by activating varied signaling pathways leading to activation of ATM and ATR activity that trigger the inhibition of RNAPI. The inhibition of RNAPI leads to the nucleolar stress response, which comprises dramatic changes in nucleolar structure, protein composition and nucleolar function [25–28]. One consequence of nucleolar rearrangement is the formation of nucleolar caps in which the FC and the DFC segregate to the exterior of the nucleolus along with rDNA. DNA repair proteins have also been identified in the nucleolar caps and it is hypothesized that the localization of repair proteins with damaged DNA aids in the repair of the rDNA [28]. The nature of the DNA damage that causes the nucleolar stress response is not known, as DSBs, acrolein and oxaliplatin induce nucleolar cap formation while cisplatin does not [29–31].

Homologous recombination (HR), non-homologous end joining (NHEJ) and nucleotide excision repair (NER) are found to occur in rDNA. HR proteins are found in nucleolar caps, suggesting

that HR occurs at these locations, while NHEJ proteins are found in the nucleoplasm [27]. Nucleolar NER is inhibited by XPC knockdown, indicating that the GG-NER pathway occurs on rDNA. However, CSB knockdown does not reduce NER, indicating that the traditional CSB-dependent TC-NER does not occur in rDNA [32].

The nucleolar DNA damage response is not limited to the repair of rDNA by these pathways. Over 4500 proteins have been found in the nucleolus including 166 DNA repair proteins [33–36]. For instance, almost half of the DNA damage response (DDR) protein poly(ADP)-ribose polymerase 1 (PARP1) is present in the nucleolus [37,38]. Mounting evidence suggests that the nucleolus is a stress response organelle that responds uniquely to different DNA damage and stressors [35]. Several proteins are released from the nucleolus upon nucleolar stress [39,40], such as PARP1, which upon release to the nucleoplasm sensitizes cells to DNA damage-induced apoptosis [38]. NPM1, a chaperone protein that is involved in ribosome biogenesis is also released into the nucleoplasm upon stress where it binds to MDM2 and prevents the MDM2-initiated degradation of p53, leading to the activation of the p53 DDR pathway [41]. Additionally, NPM1 binds to and stabilizes DNA polymerase η (Polη), increasing its activity in TLS [42].

In this study using a combination of technologies, we report the role of Polκ in the nucleolar stress response. We identified that similar to the treatment with DNA damaging agent mitomycin C or RNAPI inhibition by actinomycin D, the carcinogen BPDE causes cells to undergo nucleolar stress. During the stress nucleolar caps are formed, NPM1 is translocated from nucleolus to the nucleoplasm and the transcription of 47S pre-RNA is inhibited. Interestingly, we observe that in spite of the reduced transcription of POLK mRNA after BPDE-induced nucleolar stress, levels of Polκ remain high and enhanced Polκ activity is observed in the nucleolus. Using genetical manipulations, we gained mechanistic insight of Polk's nucleolar

activity, we demonstrated that other than Polk's TLS mechanism facilitated by binding to the PCNA ubiquination Polκ stability and activation is dependent on PARP1 PARylation and the Polycomb Repressive Complexes (PRC1) activity.

Results

TLS Polymerase κ (Polκ) is active in the nucleolus

To identify novel cellular roles of Polκ, we employed an unbiased proteomics approach to determine the proteins associated with DNA that was replicated by Polκ in cells under normal growth conditions and after exposure to BPDE. We captured the DNA replicated by Polκ by incubating cells with the novel nucleotide analog EBndG, which we previously showed to be selectively incorporated into DNA by Polκ [15]. We developed a modified aniPOND (accelerated native isolation of proteins on nascent DNA) [43] procedure, which we termed iPoKD (isolation of proteins on Pol kappa synthesized DNA), to capture proteins bound to the nascent DNA synthesized by Polκ. Two different human cell lines (HEK293 and GM12878) were treated with 0, 0.1, 0.5 or 2 μM BPDE and subsequently incubated with 100 μM EBndG. We noted that cell viability was not affected upon incubation with 100 μM EBndG (Figure S1A). The proteins bound to the DNA containing EBndG were identified by mass spectrometry. To compare the proteins associated with EBndG with proteins present at replication forks and replication-coupled DNA repair mechanisms, we complimented our iPoKD procedure with a traditional aniPOND experiment using BPDE and 5-ethynyl-2'-deoxyuridine (EdU) (Figure 1A).

A Gene Ontology (GO) analysis of our data identified many DNA replication and repair proteins previously identified with EdU pull-downs [44–46]. However, proteins associated with EBndG when compared with EdU pull-downs in both cell lines (Figure 1B, S1B) showed enrichment of nucleolar proteins required for ribosome biogenesis, processing and metabolism (Figure 1C, S1C, TableS1). Similar enrichment of nucleolar proteins was identified with Polκ synthesized DNA in U2OS human osteosarcoma cells using quantitative MS (tandem mass tag labelling) after iPoKD. Out of 511 proteins pulled-down with EBndG, 195 were nucleolar residing proteins (Figure S1D). A representation of the subset of proteins associated with nascent DNA synthesized by Polκ and their fold change compared to the beads control is shown in Figure 1D. Proteins associated with EBndG with and without BPDE damage, play roles in rDNA transcription and are present in each of the nucleolar sub-compartments (Figure 1D). The only DNA polymerase that was enriched with the iPoKD technique was Polκ. This observation supports the specificity of EBndG to Polκ and no other DNA polymerase.

BPDE exposure induced nucleolar stress and nucleolar Polκ activity

Since nucleolar proteins were enriched with the EBndG pull-down, we questioned whether Polκ is associated with the rDNA damage response pathway. To interrogate the novel role of Polκ in the nucleolus, super-resolution microscopy was used to locate and quantify EBndG in U2OS cells. These cells were utilized because they prominently display an average of 6 nucleoli per nucleus [24] and the BPDE treated S-phase arrested cells [47] show prominent DAPI-less nucleolar cavities. The incorporation of EBndG into DNA was visualized *in situ* by performing the copper(I)-catalyzed azide–alkyne cycloaddition (CuAAC) to covalently label the

EBndG with an azide fluorophore. This approach is similar to visualizing 5-EU in nascent RNA [48] or EdU in nascent DNA by the click reaction. EBndG treatment resulted in low levels of incorporation throughout the nucleus with some cells showing nucleolar incorporation (0μM BPDE panels in Figure 2A-C and S2A-D). In cells not damaged by BPDE, nucleoli were identified by regions devoid of the DAPI signal and NPM1 enriched regions as well as regions surrounding the FC and DFC detected by UBF1 and FBL, respectively (Fig 2A, C, D, E). Following increasing BPDE exposure, nucleoli were identified by regions devoid of DAPI and NPM1 and by the formation of nucleolar caps detected by FBL and UBF1. Following BPDE treatment, EBndG incorporation was increased in the nucleus (Figure 2Bii, S2C) and became noticeably enriched in the nucleolus compared with the nucleoplasm (Figure 2C-D, S2B, S2D-E). This striking observation led us to explore whether BPDE treatment caused nucleolar stress and if Polκ was involved in the DNA damage stress response in the nucleolus.

After treatment with various doses of BPDE followed by incubation with EBndG, we examined the localization of NPM1, as its translocation into the nucleoplasm is a typical hallmark of the nucleolar stress response [41]. Increasing concentrations of BPDE led to an increase in NPM1 levels (Figure 2Biii, S2C, S10A), with the protein becoming concentrated on the periphery of the nucleolus (Figure 2Ai) and at higher BPDE concentrations being totally excluded from the nucleolus (Figure 2C and S2B-D). In undamaged cells, we also observed Polκ protein as foci all throughout the cell, including in the NPM1 enriched nucleolus. However, after BPDE exposure, Polκ protein level was significantly increased (Figure 2Bi, S2Ci, S10A) with diffused Polk enrichment in the nucleolus (Figure 2C-D and S2D-E).

We next examined the nucleolar proteins UBF1 and FBL that are present in the FC and DFC, respectively, and translocate to nucleolar caps upon nucleolar stress [28]. A significant fraction of

BPDE-treated cells contained distinct large nucleoli, with rearrangement of UBF1 and FBL proteins to nucleolar caps (Figure 2D-E, S2E-F). The co-visualization of EBndG and UBF1 show the EBndG incorporation into the stressed nucleoli encircled by UBF1 (Fig 2D). Altogether, our data suggest that BPDE exposure leads to nucleolar stress.

Nucleolar stress due to DNA damage and RNAPI inhibition induces nucleolar Polκ activity

To examine if the Polκ nucleolar activity was dependent on other DNA damaging agents, we treated U2OS cells with cisplatin and mitomycin C (MMC). Polκ has been shown to protect cells against cisplatin [49,50] and MMC toxicity [51,52], possibly in repair of interstrand crosslinks. We observed that EBndG incorporation was slightly increased in cisplatin and MMC treated cells (Figure 3Aii), with enhanced accumulation in DAPI-less nucleoli (Figure 3Ai and S3A).

Nucleolar stress is not only caused by DNA damage, but also by actinomycin D, which inhibits RNAPI at low concentrations, generates fragmented nucleolus and releases several proteins from the nucleolus [53]. We questioned whether nucleolar stress caused by inhibition of rRNA synthesis could also induce nucleolar Polκ activity. Upon actinomycin D treatment, RNAPI inhibition was demonstrated by the reduced EU incorporation in the nucleolus (Figure 3Bi, iii, S3Bi) and the nucleolar stress was apparent from the NPM1 translocation from the nucleolus to the nucleoplasm and by the formation of fragmented nucleoli (Figure 3Bi,ii, S3B). Interestingly, we observed with actinomycin D treatment cellular Polκ protein and EBndG incorporation was significantly increased (Figure 3Bii, iv, v, S3B), with enhanced EBndG in

DAPI-less nucleolar regions that were devoid of NPM1 signals (Figure 3Bii, S3Bii). This result suggests that overall nucleolar stress in cells result in enhanced Polκ activity in the nucleolus.

EBndG is inserted in rDNA and its nuclear incorporation is dependent on Polκ

To confirm that the EBndG incorporation in the nucleus and the nucleolar enrichment observed after BPDE damage is entirely dependent on Polκ, we utilized U2OS sgPolK cells that were previously shown to be deficient in Polκ [54]. We observed that U2OS sgPolK cells failed to incorporate EBndG in the nucleus or nucleolus (Figure 4Ai, Aiii, S2B). We observed that even after 24 h of EBndG treatment, while the wild-type (WT) cells contained EBndG in the nucleolus, there was no trace of nucleolar EBndG in the Polκ deficient cells (Figure S4B).

In addition, we used siRNA to knockdown Polκ in U2OS cells (siPOLK) and observed significantly reduced EBndG incorporation (Figure 4Bi, 4Biii, S4A). The *POLK* transcript level was reduced by ~ 40% in siPOLK cells, and a similar decrease in *POLK* transcript level was observed upon BPDE (2 μM) treatment. The combination of siPOLK and BPDE additionally decreased *POLK* transcript levels (Figure 4C). In contrast to mRNA levels, Polκ protein level increased ~2-3 fold upon BPDE treatment. We observed that the steady state Polκ protein levels were inherently lower in undamaged cells, which was stabilized upon BPDE damage (Figure 2Bi, S2Ci, S4D). This result suggests that BPDE treatment increases Polκ levels by protecting the protein from proteolytic degradation.

In comparison to EBndG enrichment in the nucleolus that is dependent on the presence of Polκ in the cell, EdU was incorporated as foci throughout the nucleus and was not reduced in

Polκ compromised cells (Figure 4E, S4C). We also found that EBndG incorporation in the nucleolus/nucleus was not dependent on other Y-family polymerases. Cells compromised in Polη, Polι and Rev1 (transfected with respective siRNA pool) showed no reduction in EBndG incorporation (Figure 4F, S4D). Instead, we noted an increase in EBndG incorporation in Polη compromised cells (Figure 4Fii).

We next queried whether the Polκ–dependent EBndG enrichment in the nucleolus was due to the incorporation of EBndG in the rDNA. To test this possibility, we treated the cells with deoxyribonuclease I (DNase I) and observed a significant reduction in total nuclear EBndG intensity and a loss of nucleolar accumulation (Figure 5A-B, S5). Upon treatment with RNase A, we observed a small decrease in total nuclear EBndG intensity (Figure 5B), while the nucleolar pattern remained intact (Figure 5A). In contrast, while RNase H treatment did not affect the total EBndG intensity (Figure 5B), the nucleolar pattern was destroyed (Figure 5A). This result suggests that EBndG is incorporated in rDNA, possibly in regions containing R-loops.

PCNA ubiquitination is essential for Polκ nucleolar activity

To probe the mechanism by which Polκ activity is regulated in the nucleolus, we examined the role of PCNA ubiquitination that initiates the polymerase switch from a replicative to a TLS polymerase. Lysine-164 of PCNA is ubiquitinated by Rad6/Rad18 in response to replication stress induced by DNA damage or nucleotide deprivation [55,56]. The paradigm is that ubiquitination recruits TLS polymerases to the stalled replication fork [57–59]. PCNA ubiquitination is a critical regulator of Polκ recruitment and function for recovery from stalled forks after

nucleotide deprivation [8,54]. To examine the hypothesis that PCNA ubiquitination is important for Polκ activity in the nucleolus, we utilized 293T cells in which the endogenous PCNA gene was replaced by the K164R PCNA mutant [60]. We observed that upon BPDE treatment, EBndG was incorporated in the 293T-WT cells and enriched in the nucleolus as expected. However, EBndG incorporation was significantly reduced in the 293T-K164R cells (Figure 6A). This result supports the importance of PCNA ubiquitination in regulating both the nuclear and nucleolar activities of Polκ upon BPDE-induced DNA damage.

The ubiquitinated PCNA is recognized by the ubiquitin-binding zinc fingers (UBZs) present in all Y-family TLS polymerases [61,62]. Polκ contains two UBZs [63–65]. It was shown earlier that cells expressing GFP-tagged PolK (PolK-WT) but not GFP-tagged PolK with mutations in both UBZs (PolK-UBZ) interacted with ubiquitinated PCNA in cells treated with hydroxyurea [54]. To examine whether the BPDE induced nucleolar activity of Polκ is dependent on its UBZ domain, we transiently transfected U2OS sgPolK cells with either PolK-WT or PolK-UBZ. We observed that BPDE treated U2OS sgPolK cells complemented with PolK-WT rescued EBndG incorporation with nucleolar enrichment, indicating repair of rDNA. However, U2OS sgPolK cells expressing PolK-UBZ showed significantly reduced EBndG incorporation (Figure 6B, S6A). Similarly, expression of the catalytically dead mutant of PolK (PolK-CD) [54,66] (also showed reduced EBndG incorporation (Figure 6B, S6A). We also noted that the transient expression of PolK-UBZ and PolK-CD led to fragmented nucleus lacking prominent nucleoli in ~ 24% of cells imaged, unlike cells expressing PolK-WT that had oval nucleus with nucleolar patterns. The cells with distorted and fragmented nucleus showed overall high fluorescence without any distinguishable nucleolar pattern, hence we omitted those cells from our analysis (marked with arrow in Figure S6B). The observation of compromised activity of Polκ with either

UBZ or catalytic mutations, suggested that both the DNA polymerase activity and ubiquitin-mediated interactions likely through ubiquitinated PCNA are required for BPDE-induced Polκ nucleolar activity.

Polκ cellular expression and nucleolar activity are dependent on PARylation by PARP1

During DDR, one of the earliest proteins recruited is PARP1, which we found associated with EBndG on DNA newly synthesized by Polκ (Figure 1D). Approximately 40% of PARP1 molecules reside within nucleoli [38] and the binding of PARP1 to DNA induces its catalytic activity, synthesizing poly(ADP)-ribose (PAR) chains on itself, histone and non-histone proteins [67–69] that recruits DDR proteins to the DNA lesions [70]. BPDE treatment induces cellular PAR formation by PARP1 in a time and dose-dependent manner, while inhibition of PARylation by Veliparib (ABT-888) sensitizes cells to BPDE [71].

We hypothesized that the activity of Polκ, especially in rDNA, is dependent on PARP1 PARylation. We inhibited PARylation with the PARP1 inhibitor olaparib and then damaged the cells with BPDE (2μM) followed by incubation with EBndG. We found that olaparib treatment decreased EBndG incorporation in BPDE- treated cells (Figure 7A-B, S7A-B). We also noted that in olaparib-treated cells, Polκ protein expression was significantly reduced (Figure 7A-C, S7A-B). With combinative treatment of olaparib and BPDE, cells showed excessive stress, as evident by distribution of PARP1 as patches in the cytoplasm indicating that the cells were undergoing apoptosis (Figure 7A, S7A).

Recruitment of RNF2 in the periphery of the nucleolus is mediated by PARP1 PARylation and essential for Polκ's nucleolar activity

To understand the mechanism by which PARylation by PARP1 is maintaining the activity of Polκ, we probed the role of PRC proteins. There are two reasons to examine the involvement of PRCs. First, our iPokD-MS data identified the majority of the PRC canonical proteins including PRC1 protein Ring Finger Protein 2 (RNF2) as being associated with nascent DNA synthesized by Polκ (Figure 1D). Second, it was shown that recruitment of FBXL10-RNF68-RNF2 ubiquitin ligase complex (FRRUC) to DNA lesions is mediated by PARP1 and is an early and critical regulatory step in HR [72]. As we predicted, inhibition of PARylation by olaparib significantly reduced RNF2 foci throughout the nucleus, as well as the larger RNF2 discrete foci near nucleolar periphery (Figure 7Bi, 7Biv, S7B), which possibly are polycomb bodies [73]. It has already been established that PRC proteins play a role in the formation of facultative heterochromatin in the nucleolar-associated domains (NADs) located at the nucleolar periphery [74]. We observed that upon BPDE treatment, large discrete RNF2 bodies were present near the nucleolar periphery compared to untreated cells (Figure 7Bi and S4B), suggesting the presence of RNF2 in NADs. We observed enrichment of H2AK119Ub1 near the nucleolar periphery in a manner similar to RNF2 bodies (Figure S8A), consistent with RNF2-catalyzed ubiquitination in NADs after BPDE damage. This activity is known to be critical for polycomb-mediated transcriptional repression [75].

Since inhibition of PARP1 PARylation reduced the number of RNF2 containing NADs (Figure 7Bi) we examined if the nucleolar activity of Polκ is mediated by RNF2. Transfection of cells with siRNF2 significantly reduced RNF2 expression (Figure 8Ai, 8Aiv, S8B and S10D). We observed that knockdown of RNF2 reduced the Polκ levels (Fig 8Ai-ii, B, S10B) and activity

(Figure 8Ai, 8Aiii, S8B) in cells treated with BPDE. This regulation was not at the *POLK* mRNA level, as siRNF2 treatment increased POLK gene transcription without BPDE treatment (Figure 8C). Altogether, our data suggest that damage induced PARP1 PARylation increases the RNF2 foci formation that in turn maintain Polκ activity.

Polκ plays an essential role in recovering from nucleolar stress after BPDE damage

Since our experiments provide evidence that Polκ is active in the nucleolus, we next investigated whether Polκ participates in the recovery of cells from BPDE-induced rDNA damage and nucleolar stress. It was previously shown that persistent S-phase arrest in BPDE (0.1 μM) treated Polκ -/- mouse embryonic fibroblasts (MEFs), led to DSBs as detected by increased levels of γH2AX [76]. In U2OS cells, we observed a similar increase in γH2AX in undamaged Polκ compromised cells compared to cells transfected with scrambled siRNA, that profoundly increased after BPDE damage (Figure 9A, S9A). We also noticed γH2AX foci inside and in the periphery of the nucleolus, indicating DSBs in rDNA as shown by the arrows in the +BPDE panels in Figure S9A. Since rDNA damage will hinder rRNA transcription, using RT-qPCR we detected reduced 47S primary pre-rRNA transcript in BPDE treated cells (Figure 9B). Surprisingly, we observed reduction in pre-rRNA transcription in Polκ compromised cells (Figure 9B). In addition, we incubated cells with 5-ethynyluridine (EU) to examine rRNA transcription in the nucleolus. As expected, we observed robust nucleolar EU incorporation in cells (Figure 9C and S9B), indicating rRNA transcription. However, EU incorporation was significantly reduced in Polκ compromised cells (Figure 9C and S9B), as well as in Polκ deficient U2OS sgPolK cells (Figure 9D and S9C). Upon complementation of U2OS

sgPolK cells with GFP-PolK WT, even after BPDE treatment the EU incorporation was rescued with nucleolar EU enrichment, indicating recovery of rRNA transcription (Figure 9D and S9C). These experiments suggest that Polκ is important for repairing BPDE-induced rDNA damage and resuming rRNA transcription. Interestingly, our data also indicates Polk's role in the rRNA transcription.

We next examined whether Polκ participates in the recovery from BPDE-induced nucleolar stress. We treated Polκ wild-type and knockdown cells with 0.5, or 2 μM BPDE for 2 h, then fixed the cells immediately (t=2 h) or allowed them to recover for 36 h in growth media (t=36 h) (schematic in Figure 9E). As observed before (Figure 2C), wild-type cells at t=2 h showed NPM1 translocated from the nucleolus to the nucleoplasm. After 36 h of recovery, NPM1 partially returned to the nucleolar periphery. However, BPDE-treated Polκ compromised cells, NPM1 redistributed throughout the cell with a majority of NPM1 in the cytoplasm (Figure 9F, S9D, S2B). Although Polκ expression in the siPOLK cells was recovering after 36 h due to the exhaustion of the siRNA, the recovery from nucleolar stress is still impaired (Figure 9F, S9D).

To further examine the role of Polκ in recovering from nucleolar stress, we examined the formation and recovery of nucleolar caps. As illustrated in Figure 9G, treatment of 0.5 μM BPDE led to the translocation of UBF1 from the interior of the nucleoli to the periphery, an indication of nucleolar cap formation, in both siScrambled and siPOLK cells after 2 h. After 36 h, UBF1 returned to the nucleolus in siScrambled cells, while Polκ compromised cells retained UBF1 in the nucleolar caps (Figure 9G, S9E). This result supports a role of Polκ in the recovery from BPDE-induced nucleolar stress.

Discussion

We demonstrated that the Y-family TLS polymerase Polκ is active in the nucleolus. The nucleolar activity of Polκ is profoundly increased upon nucleolar stress induced by DNA damage and inhibition of rRNA synthesis. We also found that Polκ protected the cells from nucleolar stress (Figure 10). This conclusion relies on two independent experimental approaches. First, by establishing a novel tool, iPoKD-MS, nucleolar proteins were surprisingly discovered to be highly enriched in DNA that had been synthesized by Polκ. Second, by using super-resolution confocal microscopy, the presence and activity of Polκ in the nucleolus was found to be increased after exposure to BPDE, cisplatin, MMC and actinomycin D.

The initial damage produced by BPDE is primarily the N^2-BP-dG adduct, but these bulky adducts led to DSBs as shown by an increase in γH2AX [76,77](Figure 9). Cisplatin and MMC form mono adducts as well as DNA interstrand crosslinks (ICLs) [78,79]. Actinomycin D does not form a covalent bond with DNA but intercalates with GC-rich regions, such that low concentrations preferentially inhibit RNAPI-dependent transcription as the promoter of 45S ribosomal gene is GC-rich [80]. Although the mechanism of DNA damage varies, these agents induce nucleolar stress. Actinomycin D enlarges the cell nucleus while diminishing and breaking apart the nucleoli [53]. We showed that BPDE treatment induced the nucleolar stress response by the formation of nucleolar caps (Figure 2), the release of NPM1 from the nucleolus into the nucleoplasm (Figure 2) and inhibition of RNAPI transcription of pre 47S rRNA (Figure 9). It is not clear whether the N^2-BP-dG adduct or the induced DSBs led to the nucleolar stress response. MMC and cisplatin also inhibit rRNA synthesis causing nucleolar stress [81–83].

Using the specificity of EBndG for Polκ, we showed that Polκ has activity to some extent in all cells, thus is not cell-cycle dependent and may accompany a DNA repair process. Cells are constantly exposed to endogenous damage [84] and the EBndG incorporation may be related to its NER [9] or cross-link repair [10,11] activity. Despite the observation that Polκ activity is dependent on PCNA ubiquitination and the Polκ UBZ domain (Figure 6), the majority of the Polκ activity is not due to TLS bypass during S-phase. Thus, we conclude that Polκ is active in the nucleolus during nucleolar stress generated by rDNA damage and inhibition of rRNA transcription.

Incubation of EBndG-treated cells with DNase I and RNase A indicated that the primary site of EBndG incorporation is DNA. The loss of the nucleolar signal with RNase H treatment suggests an association with R-loops in which hydrolysis of the RNA allowed the DNA-bound EBndG to diffuse throughout the nucleus (Figure 5). R-loops are transient, reversible structures that form in many regions of the genome. Predictors of R-loop presence include high transcriptional activity, open DNA and high GC content, all present in rDNA [85,86]. R-loops participate in the regulation of transcription, but they also represent a potential source of damage, and their presence must be carefully regulated [87]. The regulation of R-loops depends on RNA-methylation, including METTL3/14 dependent 6-methyladenine (m^6A) and METTL8 dependent 3-methylcytosine formation [88–90]. m^6A RNA was shown to selectively recruit Polκ to UV-damage sites to facilitate repair [91] . Thus, Polκ may interact with nucleolar R-loops.

Since BPDE damage induces transcription arrest at the sites of damage [92] as well as genome-wide [93,94], we found that the level of *POLK* mRNA was reduced after BPDE treatment (Figure 4C). However, we observed that the Polκ protein level was increased (Figure 4D). The half-life

of Polκ is 5 hours [95], thus the reduced *POLK* mRNA should lead to lower Polκ levels unless the protein is stabilized. Our finding that the activity of Polκ did not decrease over 36 hours therefore suggests that Polκ protein was stabilized (Figure 9). NPM1 has been shown to regulate TLS by preventing proteasomal degradation of DNA Polη [42]. It is possible that NPM1's upregulation and translocation into the nucleoplasm in BPDE-exposed cells helps in maintaining Polκ protein stability, increasing its activity in maintaining genomic stability and thus promoting cell survival. Upon BPDE damage, while there was some increase in nuclear activity of Polκ, there was a huge increase of the activity of Polκ in the nucleolus as detected by enriched EBndG incorporation. Although Polκ was not detected in the nucleolar proteome [33,96], we observed increased Polκ levels in the nucleolus after BPDE damage (Figure 2C, S2D). Thus, we postulate that carcinogens causing nucleolar stress stabilizes Polκ protein in the cell with an increased localization in the nucleolus leading to higher nucleolar activity. Down regulation of Polκ resulted in BPDE sensitivity, with an increase in DSBs, reduced rDNA transcription as well as nucleolar EU incorporation. Additionally, the cells with Polκ were able to respond to BPDE-induced nucleolar stress more rapidly than Polκ deficient cells (Figure 9). These findings emphasize that Polκ plays critical role in recovering after BPDE-induced cellular and nucleolar stress.

Enrichment of PARP1 and the canonical PRC proteins in the iPoKD-MS data, led us to examine their involvement in the activity of Polκ (Figure 1D, Table S1). Our data identified PARylation by PARP1 and the presence of RNF2, the E3 ubiquitin ligase in the PRC1 complex, were required to maintain Polκ levels and its activity in the nucleus/nucleolus (Figures 7 and 8). We noted PARP1 in the cytoplasm of cells treated with both olaparib and

BPDE. This result suggests that ablation of PARylation led to the inability of cells to respond to BPDE-induced damage by triggering the apoptosis pathway, in which the caspase fragmentation of PARP1 produces a smaller PARP1 fragment that translocates to the cytoplasm and induces apoptosis [97].

Lack of PARylation also reduced RNF2 foci formation (Figure 7B). When PARylation is inhibited and RNF2 is down regulated, the Polκ levels decreased with a consequent decrease in activity. The effect of RNF2 is complex, because siRNF2 cells showed an increased *POLK* transcript but a decreased Polκ protein level. Since Polycomb proteins including RNF2 has been indicated to play roles as both transcriptional repressor and activator, we speculate that RNF2 regulates a protein that stabilizes Polκ, thus RNF2-deficient cells showed decreased Polκ.

In summary, our data suggest that BPDE exposure leads to genomic lesions including rDNA damage that trigger nucleolar stress. During the nucleolar stress response, nucleolar caps forms as foci to repair damaged rDNA, NPM1 expression increases and translocates to the nucleoplasm, potentially enhancing Polκ protein stability and its activity in the DNA repair process. We show Polκ nucleolar activity is increased upon nucleolar stress generated by treatment with DNA damaging agents BPDE, cisplatin and MMC, as well as the RNAPI inhibitor actinomycin D. The BPDE-induced DNA lesions induced PARP1 activity that promoted polycomb body formation near nucleolar periphery, which potentially induces facultative heterochromatin regions at the NADs to promote inhibition of rDNA transcription. The activity of Polκ was critical in recovering cells from BPDE-induced nucleolar stress and S-phase arrest. In addition, Polκ's binding to ubiquitinated PCNA and Polκ's catalytic domain are

important for its BPDE-induced nuclear/nucleolar activity. Thus, in our study, we identified the novel role of Polκ in repairing damaged rDNA, resuming rRNA synthesis and recovering from nucleolar stress caused by BPDE. Our findings provided mechanistic insight of Polκ's activity that is dependent on PARP1 PARylation and PRC protein other than its TLS mechanism (Figure 10). This study opens a new direction raising several questions: whether NPM1 directly regulates Polκ's stability, how RNF2 facilitates Polκ protein stability and how Polκ regulates rRNA transcription. Since recent evidence connect nucleolar stress as a hallmark in a variety of cancers, neurological and aging-associated diseases [73,73–75], our report demonstrating the critical role of Polκ in nucleolar stress recovery and rDNA maintenance reveal new therapeutic strategies for multiple disease conditions.

Methods

Cell culture, drug treatments and plasmid transfection

HEK293, 293T-K164R [60], U2OS and U2OS sgPolK [54] cell lines were cultured in Dulbecco's modified Eagle medium (DMEM), supplemented with 10% fetal calf serum (FCS), GM12878 cells were cultured in Roswell Park memorial Institute (RPMI) 1640 medium with 15% FCS. Both the media contained 2mM L-glutamine and penicillin–streptomycin antibiotics and cells were grown under standard cell culture conditions in a CO_2 incubator (37 °C; 5% CO2). BPDE stock (obtained from the Organic Synthesis Core of the Penn State Cancer Institute) was diluted in DMSO concentrations to prepare 0.1, 0.5 or 2 μM from stock by diluting and added immediately to the media. The cells with BPDE added media were incubated for 2 hours in a CO_2 incubator. For olaparib treatment, cells were incubated for 72 hours with 4 μM olaparib

(Sigma-Aldrich, gift from George Lucian Moldovan's lab) added to DMEM. BPDE damage for 2 hours was performed in 72 hours of olaparib treated cells. For MMC and cisplatin treatment, U2OS cells were incubated with either 30 μM mitomycin C (dissolved in DMSO), 10 μM cisplatin (dissolved in 0.9% NaCl), or the solvent controls for 2 hours. For actinomycin D treatment cells were incubated with 5 nM actinomycin D or DMSO for 6 hours.

Transient plasmid WT-PolK GFP [54] transfections were performed using FuGene six reagent (Promega), according to manufacturer's instructions. Analyses were done between 24–48 h after plasmid transfection.

Isolation of protein on nascent Polκ synthesized DNA (iPoKD)

This procedure is a modification of the native iPOND procedure [98]. GM12878 cells (~8X10^6) after treatment with 0, 0.5 μM or 2 μM for 2 hours were incubated with 20 μM EdU (15 min) or 100 μM EBndG (30 min) and harvested by centrifugation at 200xg for 7.5 mins. HEK293 cells (~4-6x10^8) were incubated after BPDE damage with EdU (15 min) or EBndG (180 min). U2OS cells were incubated after 2 μM BPDE damage 100 μM EBndG for 30 mins and immediately harvested (sample "Pulse"). From another set the media containing EBndG was removed and fresh media added and incubated for 180 min then harvested (sample "Wash-Chase"). Sample for "Beads control" had no nucleotides (EdU or EBndG) added to the cells. Pellets were resuspended in 10 mL of pre-chilled freshly prepared NEB (20mM HEPES-KOH pH 7.2, 50mM NaCl, 3mM MgCl2, 300mM sucrose, 0.5% NP 40 substitute or TX100) and rotated at 4°C for 15 mins. The nuclei were pelleted by centrifugation for 10 min at 500xg at 4°C to pellet. The nuclei pellets were resuspended in 10 mL ice-cold PBS with a serological pipette to wash (10

μL used to check the nuclei under microscope) and collected by centrifugation at 500×g for 10 min at 4°C. The nuclei pellets were completely resuspended in 10 mL of freshly prepared click reaction mixture [1 mM CuSO4, 2 mM tris(3-hydroxypropyltriazolylmethyl)amine (THPTA), 10 μM azido-PEG3-biotin (Alfa Aesar #J 64996) 10 mM sodium ascorbate, complemented with PBS] and incubated for 1.5 hours at room temperature (RT). The nuclei were centrifuged for 10 min at 500xg at 4°C and the pellet washed 3X with 10 mL ice-cold PBS. The nuclei pellet was either immediately frozen in liquid nitrogen and kept in -80°C or were immediately lysed as described below.

The nuclei pellets were resuspended in 0.5 mL of ice-cold freshly prepared buffer B1 (25 mM NaCl, 2 mM EDTA, 50 mM Tris-HCl-pH8, 1% NP-40 substitute or TX100) supplemented with protease inhibitors (Roche cOmplete Protease Inhibitor Cocktail) and transferred to a 1.5 mL tube and rotated at 4°C for 30min. The nuclei were pelleted by centrifuged at 500xg for 10 mins at 4°C supernatant saved as low soluble chromatin and nucleoplasm fraction. The pellets were resuspended again in 0.5 mL of ice-cold buffer B1 and rotated at 4°C for 30 min. The chromatin was solubilized with a microtip sonicator (Fisher Scientific Model 500 Sonic Dismembrator) by keeping the tubes on ice and performing 6 rounds of 2 X10s on, 10s off (~20A with 1min Rest output). The samples were centrifuged for 10 min at 16100xg at 4°C and the solubilized chromatin fraction was collected. An aliquot was saved as an input sample. The rest of the sample was supplemented to 1 mL with ice-cold buffer B1 containing protease inhibitors, 50 μL of MyOne Streptavidin T1 Dynabeads (MyOne Streptavidin T1 65602, Thermo-Fisher) were added, and rotated overnight at 4°C. The beads were washed 6 times with buffer B1. The protein was eluted by boiling in 1X Laemmli buffer.

Mass Spectrometry and Proteomics data analysis

The eluted proteins were loaded on a 10% SDS-PAGE gel, resolved for approximately 5mm, and Coomassie stained. Gel bands containing the protein samples were excised from the gel, reduced using 3 mM tris(2-carboxyethyl)phosphine (TCEP) in 100 mM ammonium bicarbonate, and cysteine residues were alkylated using 3 mM 2-carboxyethyl methanethiosulfonate (CEMTS). Proteins were then in-gel proteolyzed using Sequencing grade modified porcine trypsin (Promega), and peptides were eluted (80% acetonitrile, 1% TFA) and lyophilized. Peptides were resuspended in 30 μL 0.1% aqueous formate, and 2 μL of solution were used for LC/MS analysis. Using an easyLC1200 nano-chromatograph (Thermo Scientific), peptides were loaded on a 20 cm x 75 μm ID column packed in house with Reprosil C18 silica particles (1.9 μm diameter, Dr. Maischt), and resolved on a 5-35% acetonitrile gradient in water (0.1% formate) at 250 nl/min.

Eluting peptides were ionized by electrospray (2000 V) and transferred into a Thermo Lumos Orbitrap mass spectrometer whose ion transfer tube was maintained at 305 ^{o}C. The MS was set to collect 120,000 resolution orbitrap precursor scans (profile mode) every 3 s (m/z 380-2000 Da, AGC= 400,000 ions, maximum injection time = 50 ms, RF lens = 30%). Precursor ions were selected for data-dependent acquisition in cycle-time mode (i.e. performing as many MS2 as possible within the 3 s interval between consecutive MS1 scans), applying the following filters: dynamic exclusion 30 s with 10 ppm mass tolerance, monoisotopic ion selection based on isotopic pattern expected for peptides, charge state 2-7 (ions with undetermined charge state were excluded), and minimum ion intensity 5,000. Precursor ions were selected using the quadrupole (isolation window = 1.2 Da), accumulated for up to 50 ms (AGC= 30,000 ions), and fragmented by HCD at stepped 26,32,38% normalized energy.

Spectra were recorded in centroid mode using the linear trap at “normal” (unit) resolution, with first mass locked to 100 Da. The reversed phase column was washed after each sample injection to prevent carry over.

Files searched using the Mascot scoring function within ProteomeDiscoverer v.2.4, with mass tolerance set at 5 ppm for MS1, and 0.5 Da for MS2. Spectra were matched against the UniProt human database (as of January 2021, containing 40,967,805 residues and 101,014 protein sequences) and a database of common contaminants (cRAP). M-oxidation, and N/Q-deamidation, were set as variable modifications. CEMTS adduct on cysteine was set as fixed modification. Trypsin was set as protease with up to 3 missed cleavages allowed. Peptide-spectral matches were filtered to maintain FDR<1% using Percolator. Extracted ion chromatograms of precursor ions intensities were integrated for label-free quantification (LFQ_ across samples and used as quantitative metric for protein relative quantification.

Proteins with peptide count 2 and above were further analyzed. The ribosomal proteins (RPL proteins) were removed from all data sets as they are highly expressed in all cells. The abundance value of each protein that are pulled down by either EdU or EBndG were divided by the abundance value of beads control to attain the fold change (FC). To permit calculation of LFQ ratios for proteins with missing values in the bead controls, an arbitrary value (2222, chosen to be slightly smaller than the lowest empirical value) was used for imputation. The FC was further calculated as log base 2, and proteins that have FC log2 = 1 and higher are considered as the final number of proteins pulled down. EdU pull-down were compared with the EBndG pull-down proteins that were represented in Venn diagrams. The GO analysis of the unique EdU and EBndG-associated proteins were analyzed by ToppGene. The full ToppGene analysis were shown in Table S1.

The U2OS cells iPoKD samples in-gel digested as described above, replacing ABC buffer with Triethylammonium bicarbonate buffer (TEAB), and encoded with 10-plex Tandem Mass Tag (TMT) according to manufacturer's protocol (Thermo Fisher). After quenching the TMT reagent with 5% hydroxylamine, TMT-labelled samples were pooled, lyophilized by vacuum centrifugation, and fractionated by C18 Reversed Phase chromatography in spin column format at pH 9. Eluates were acidified with 0.1% TFA, lyophilized, and reconstituted in 30 μl 0.1% aqueous formate. 3 μl of each fraction was analyzed in duplicate by LC-MS. Labelled peptides were resolved using an easyLC1200 nano-chromatograph (Thermo Scientific), peptides were loaded on a 25 cm x 75 μm ID column packed in house with Reprosil C18 silica particles (1.9 μm diameter, Dr. Maischt), and resolved on a 5-35% acetonitrile gradient in water (0.1% formate) at 200 nl/min. Eluting peptides were ionized by electrospray (2200 V) and transferred into a Thermo Exploris Orbitrap mass spectrometer whose ion transfer tube was maintained at 275 ^{o}C. The MS was set to collect 120,000 resolution orbitrap precursor scans (profile mode) every 3 s (m/z 380-2000 Da, AGC= 400,000 ions, maximum injection time = 50 ms, RF lens = 40%). Precursor ions were selected for data-dependent acquisition in cycle-time mode (i.e. performing as many MS2 as possible within the 3 s interval between consecutive MS1 scans), applying the following filters: dynamic exclusion 30 s with 10 ppm mass tolerance, monoisotopic ion selection based on isotopic pattern expected for peptides, charge state 2-5 (ions with undetermined charge state were excluded), and minimum ion intensity 1,000. Precursor ions were selected using the quadrupole (isolation window = 1.2 Da), accumulated for up to 110 ms (AGC= 30,000 ions), and fragmented by HCD at stepped 26,32,38% normalized energy. Spectra were recorded in centroid mode using the orbitrap at 60,000 resolution, with first mass locked to 100 Da.

Peptide-spectral matching and reporter ion intensity extraction were performed using Proteome Discoverer v2.4, with Mascot as scoring function set as above except for MS2 mass tolerance set to 20 ppm, and TMT10-plex adduct set as fixed modification. The Abundance of each protein identified in "Pulse" and 'Wash-Chase" samples were normalized with "Beads Control". The "Pulse"/"Wash-Chase" proteins with peptide count 2 and above were used for ToppGene analysis.

RNA transfection and Real-time PCR

Gene knockdown was performed using Lipofectamine RNAiMAX transfection reagent according to the manufacturer's protocol. The cells were harvested after 72 hours for RNA isolation using Zymo Research RNA isolation kit. cDNA prepared using SuperScriptIII Reverse Transcriptase kit (Thermo Fisher) and OligodT primers. To check for the transcript level of pre-rRNA the cDNA was synthesized using random hexamer primers. Realtime PCR was performed using 10 ng of cDNA with SYBR Green Master mix. Samples were analyzed on a LightCycler480 and quantified with LightCycler480 quantification software. The fold change calculated by delta-delta Ct method with GAPDH as the housekeeping gene control. The primers used are:

GAPDH primers (5'CGACCACTTTGTCAAGCTCA3' and 5'AGGGGAGATTCAGTGTGGTG3'), 47S pre-rRNA (5'TGTCAGGCGTTCTCGTCTC3'

and 5'GAGAGCACGACGTCACCAC3'), POLK [77](5'TGAGGGACAATCCAGAATTGAAG 3' and 5'CTGCACGAACACCAAATCTCC)

SDS-PAGE and western blotting

Cells were harvested and lysed in lysis buffer (50mM Tris pH8, 20mM NaCl, 10mM MgCl2, 0.1% SDS, EDTA-free Protease Inhibitor-Roche), centrifuge for 10 min and supernatant collected. Proteins were quantified by nanodrop and boiled in Laemmli buffer. Proteins were separated with 4–20% Precast SDS–PAGE gels (Biorad #4561093), transferred to PVDF membranes and were blocked with 5% milk in TBS-T buffer. Bands were detected using various antibodies at 4°C overnight. The membranes were incubated with peroxidase-conjugated secondary antibodies for 1 hour at RT before detection using ECL system. For Polκ detection supersignal west pico PLUS chemiluminescent was used (ThermoFisher). Images captured with ChemiDoc imaging system (Biorad), and the bands quantified using ImageJ with either GAPDH or vinculin as control. All the uncropped versions of images were showed in Supplementary Figures.

Immunofluorescent staining and click fluorophore labelling

Cells were grown overnight on glass coverslips coated with poly-D lysine. After 2 hours treatment with either DMSO or variable concentration of BPDE diluted with DMSO (0.1 to 2μM), fresh media was added with either 5-EU (1 mM for 1 h) [48], EdU (20 μM for 10 min) or EBndG (100 μM for 30 min) and the control with DMSO for 30 mins. The cells were gently washed 2x with PBS and fixed with 4% buffered paraformaldehyde at room temperature (RT) for 20 min. Cells were washed twice with PBS containing 1% BSA or kept in 1% BSA overnight at 4°C, then permeabilized with 0.5% (v/v) Triton X-100 in PBS for 15 min. Cells were washed with PBS and click fluorophore labelling was performed by incubating with click reaction 1 mM

CuSO4, 2 mM THPTA, 10 mM sodium ascorbate, 0.2 μM Alexa Fluor 594 azide (Thermofisher A10270) complemented with PBS for 1.5 hours at RT in dark. The cells were washed 3x with PBS and incubated in blocking buffer containing 10% donkey serum (JacksonImmunoResearch 017-000-121) in PBS for 1 hour, washed with PBS and incubated with primary antibody solution in 1% blocking buffer overnight at 4C. Cells were then washed 3x with PBS and incubated with secondary antibody solution, consisting of 1: 2000 (v/v) donkey anti-mouse Alexa Fluor 647 (A-31571) or donkey anti-rabbit Alexa Fluor 488 (A-21206) for 2 hours at room temperature. Washed 3x with PBS followed by 5 min incubation in 4′,6-diamidino-2-phenylindole DAPI (1:2000) and mounted with Vectrashield mounting medium.

RNase A, RNase H and DNase I digestion

U2OS cells grown on coverslips overnight were treated either with DMSO or 2 μM BPDE for 2 hours, then incubated with fresh media with only DMSO (no nucleotide control) or 100 μM EBndG for 30 minutes. After washing with PBS, cells were incubated for 15 min either with PBS (control) or DNase I (10U) (NEB M0303) or RNase A (2mg/mL) (NEB T3018) or RNase H (NEB M0297) at 37C, fixed in 2% paraformaldehyde for 20 minutes and incubated in blocking buffer (1% BSA in PBS). Cells were permeabilized and click reaction performed for 1.5 hours as described above. Cells were again incubated with either PBS (control) or DNase I or RNase A or RNase H for 15 minutes, followed by two more washes with PBS buffer. Cells were further processed for immunofluorescence as described above.

Confocal Microscopy, Image Analysis, Quantification and Statistical analysis

Imaging was performed by super resolution confocal microscopy using Zeiss LSM910 with AiryScan2 in multiplex mode SR-2Y using a 20X (NA 0.8), 40X (NA 1.2) water and 63X oil (NA 1.4) objectives. Imaging parameters such as laser power, digital gain, digital offset, scan speed was kept constant for the same experimental batch of treated and untreated cells. Resulting images were quantified through a custom image analysis pipeline using CellProfiler version 4.2.1 [99]. Briefly, individual imaging channels were first split for object detection. In all images DAPI channel was used for nuclei object detection. RNF2 foci was identified as an independent object within each nuclei and related to the original nuclei object as a child object using relate object function. The nuclei objects were further used as masks on EBndG, EdU, EU, PolK, UBF1 and γ-H2AX channels using the image mask function to isolate and measure the intensity within the individual nuclear object boundaries. The RNF2 foci counts, and fluorescence intensities of EBndG, EdU, EU, Polκ, UBF1 and γH2AX were exported as spreadsheet for statistical analysis using GraphPad Prism version 10 software. In box plot graphs, boxes represent the 25–75 percentile range with median, and whiskers represent the 5–95 percentile range. Statistical tests were applied as described in the Figure legends and were calculated with Prism 9. In all quantitative immunofluorescence studies, random cells per group were scored and mentioned in the figure legends.

Cell viability assay

Cell viability was determined using the CellTiter-Glo® 2.0 Luminescent Cell Viability Assay. Briefly, U20S cells were seeded in a 96-well plate (2,000 cells/well) and allowed to adhere overnight. The following day, cells obtained varying concentrations of EBndG or DMSO in

triplicate and were incubated for 3 days. On day 3, CellTiter-Glo® Reagent was added at half the volume of cell culture media present in each well. Plates were rocked for 2 minutes and then incubated at RT for 10 min and analyzed with a luminometer (GloMax® Navigator Luminometer). Background signal from the media and CellTiter-Glo® Reagent control was subtracted from sample values. To ensure the CellTiter-Glo® Reagent was not oversaturated with ATP in the sample wells, 1 mM ATP disodium salt was used to evaluate the luminescent value near saturation.

List of antibodies used:

anti-POLK or anti-DinB (sc-166667, IF 1:100, WB 1:1000), anti-POLH (sc-17770, IF 1:100), anti-POLI (sc-101026, IF 1:100), REV1 (sc-393022, IF 1:100), anti-RNF2 (Bethyl laboratories A302-869A, IF 1:1000, WB 1:5000), anti-PARP1(gift from George Lucian Moldovan lab, Ab-95425 IF1:500), anti-NPM1 (HPA011384 Sigma, IF 1:250, WB 1:2500), anti-UBF1 (sc-13125, IF1:100), anti-FBL (ab137422 IF 1:250), anti-H2K119ub (gift from Zhonghua Gao lab, Millipore D27C4 IF 1:1600), anti-γH2AX (sc-517348, IF 1:150), anti-GAPDH (Invitrogen 39-8600 WB 1:2500) , anti-vinculin (gift from George Lucian Moldovan lab sc-73614, 1:1000)

Secondary antibody used with anti-DinB is m-IgGκ BP-HRP (sc-516102).

List of siRNA used:

siRNF2 [79], siPOLK (pool of 3 siRNAs sc-60537), siScrambled (santa cruz), pool of 3 custom made Dicer-Substrate Short Interfering RNAs (DsiRNAs) from IDT.

Figure Legends

Figure 1. EBndG-bound proteins enriched in the nucleolus, ribosomal biogenesis and in transcriptional repression.

A. Experimental design to identify proteins enriched at nascent DNA synthesized with Polκ captured by EBndG (iPoKD) compared to traditional aniPond. Chemical structures of EdU and EBndG shown.

B. Venn diagrams depicting number of proteins associated with EdU (green) compared to EBndG-pull downs (red) using GM12878 cells. EdU-pull down in untreated cells identified few unique proteins (25) and were not analyzed by ToppGene Suite.

C. GO analysis (ToppGene) of EdU and EBndG-bound unique proteins (non-overlapping protein list from venn diagrams in Fig1B analyzed). Gene counts from each pathway shown in the graph and the p-value for each pathway is indicated within each bar. EdU (green) and EBndG-pull downs (red) from cells treated with 0, 0.5 and 2 μM BPDE. See Table S1 for complete results.

D. Representative list of proteins bound to Polκ synthesized DNA and their fold change compared to the beads control. The protein list of the EBndG-pull downs from HEK293 cells treated with 2 μM BPDE and GM12878 cells treated with (0, 0.5 and 2 μM) BPDE were analyzed with their respective beads control. Proteins grouped according to their known interacting protein complex and presence in nucleolar sub-compartments.

Figure 2. BPDE exposure induces nucleolar stress and increases the activity of Polκ in the nucleolus

A. **(i)** Representative images of U2OS cells from *N* = 2 independent experiments showing EBndG (red), NPM1 (gray) and DAPI (blue). EBndG (red) in DAPI-less regions and NPM1 in the nucleolar periphery (shown with arrows) in cells after BPDE treatment (0.1 μM).

(ii) Quantification of nuclear EBndG intensity in untreated (n=103) and BPDE-treated (n=63) cells, represented as box plots. Boxes represent the 25–75 percentile range with median and whiskers represent the 5–95 percentile range. Data points outside of this range are shown individually. Statistical significance calculated using two-tailed Mann Whitney U test. * P = 0.0192

B. Quantification of total nuclear (i) Polκ, (ii) EBndG and (iii) NPM1 intensity, in 30-60 untreated and 0.5 μM BPDE-treated cells represented as box plots. Statistical analysis as Figure 2Aii. **** P <0.0001. Full images shown in Figure S2B.

C. Representative images of untreated and BPDE-treated (2 μM) cells from *N*=3 independent experiments (quantitation in Figure S2C and full z-stack in Figure S2D). Nucleus shown by DAPI (blue), NPM1 (gray) enriched in nucleolus and nucleolar periphery in untreated cells, whereas excluded from nucleolus and present in the nucleoplasm in BPDE-treated cells. A few nucleoli are marked with arrows. Overlay panel of Polκ (green) and NPM1 shows presence of Polκ foci in the nucleoli (inset **i,ii**). DAPI and EBndG overlay with prominent EBndG enriched (red) in all DAPI-less nucleoli. Full image shown in Figure S2C.

D. Representative images of untreated and BPDE -treated (2 μM) cells from *N* = 2 independent experiments. Untreated cell with UBF1 (green, shown with an arrow) in nucleoli

and after BPDE treatment, UBF1 in the nucleolar caps (green, shown by arrows). The EBndG enriched nucleoli shown in red. Full images shown in Figure S2D.

E. Representative cells showing FBL (magenta foci) with UBF1 (green) in nucleolar caps (shown by arrows) following BPDE treatment (2 μM). Full images shown in Figure S2E.

All scale bars = 10 μm.

Figure 3: Nucleolar stress induced by cisplatin, mitomycin C and actinomycin D increases the activity of Polκ in the nucleolus

A. (i) Representative images of DMSO, cisplatin and mitomycin C-treated cells with EBndG (red). Overlay of DAPI (blue) and EBndG, with nucleolar enriched EBndG (red with an arrow) Full images shown in Figure S3A.

(ii) Quantification of nuclear EBndG intensity in DMSO (n=67), cisplatin (n=125), mitomycin C (n=59) -treated cells, represented as box plots. Statistical significance calculated using Kruskal -Wallis test. *P = 0.0045. All scale bars = 10 μm.

B. (i) Representative images of DMSO and actinomycin D-treated cells with Polκ (green), EU (red), NPM1 (gray). Overlay of DAPI (blue), NPM1 and EU shows EU in nucleolus in untreated cells (as shown by an arrow).

(ii) Representative images of DMSO and actinomycin D-treated cells. Overlay of DAPI (blue), NPM1 and EBndG, with nucleolar enriched EBndG (red with an arrow) in actinomycin D-treated cells. Full images shown in Figure S3B. All scale bars = 10 μm.

(iii-vi) Quantification of nuclear EU (~25 cells), and nuclear EBndG, Polκ and NPM1 intensity in 150-160 DMSO and actinomycin D-treated cells represented as box plots. Statistical analysis as Figure 2Aii. **** P <0.0001, * P <0.0226.

Figure 4: Polκ dependent incorporation of EBndG in the nucleus and nucleolus

A. **(i)** Representative images of wild type (WT) U2OS and U2OS sgPolK cells (Polκ -/-) treated with BPDE (0.5 μM). WT cells showing Polκ (green) and nucleolar enriched EBndG (red). BPDE-treated cells with NPM1 (gray) in the nucleoplasm.

(ii) Quantification of total nuclear Polκ, NPM1and EBndG intensity in wild-type (WT) (n=63) and Polκ -/- cells (n=47), represented as box plots. Statistical analysis as 2Aii. **** P <0.0001, *** P <0.0004, * P <0.0193. Full image shown in Figure S2B.

B. (i) Representative images of cells transfected with siScrambled and siPOLK, showing EBndG (red, nucleolar EBndG shown by arrows), Polκ (green), and DAPI (blue).

(ii) Quantification of total nuclear Polκ and EBndG intensity of siScrambled (n=80) and siPOLK (n=74) transfected cells, represented as box plots. Statistical analysis as Figure 2Aii. **** P <0.0001. Full image shown in Figure S4A.

C. Relative expression of POLK transcript in siScrambled (siSc) and siPOLK transfected cells after treatment with 0 and 2 μM BPDE. GAPDH mRNA as internal control. Calculated with the comparative CT method (mean ± SEM). All comparisons are relative to siSc 0 μM BPDE.

D. Western blot analysis of Polκ expression in siSc and siPOLK transfected cells, after treatment with 0 and 2 μM BPDE. Fold change (FC) of Polκ after normalization with vinculin and compared to siSc (BPDE=0). Full blots in Figure S10B.

E. (i) EdU (red) incorporation in WT and Polκ -/- cells, after treatment with 0 and 0.5 μM BPDE, DAPI (blue).

(ii) Quantification of nuclear EdU intensity in 0 μM BPDE-treated cells [WT (n=102) and Polκ-/- (n=103)], 0.5 μM BPDE-treated cells [WT (n=56) and Polκ -/- (n=82)]. Results represented as box plots. Statistical significance calculated using the Kruskal-Wallis ANOVA test. Full image in Figure S4C.

F. (i) Representative images of cells and **(ii)** their nuclear EBndG intensity quantification. Cells were transfected with siScrambled (n=45), siPOLι (n=29), siPOLη (n=46), siREV1(n=49). Nucleolar EBndG (red, shown by arrows) and DAPI (gray). Statistical analysis as Figure 4Eii. **** P <0.0001, * P <0.0178. Full image in Figure S3F.

All scale bars = 10 μm.

Figure 5: EBndG incorporation in nucleolar DNA

A. Representative images of BPDE-treated (2 μM) cells from *N* = 2 independent experiments showing EBndG (red) enriched nucleolus, Polκ expression (green), NPM1 in the nucleoplasm (gray) and DAPI (blue) followed by either treatment with buffer, RNase A, RNase H or DNase I.

B. Quantification of nuclear EBndG intensity in cells treated with buffer (n=177), RNase A (n=203), RNase H (n=236) and DNase I (n=214) represented by box plots. Statistical analysis as Figure 4Eii. **** P <0.0001. Full image in Figure S5. Scale bar = 10 μm.

Figure 6: PCNA ubiquitination dependent activity of Polκ

A. (i) Representative images of BPDE-treated (0.5 μM) wild type (293T-WT) and PCNA K164R mutant (293T-K164R) cells. Overlay of DAPI (blue) and EBndG showing nucleolar EBndG (red) enriched nucleolus in 293-WT cells.

(ii). Quantification of nuclear EBndG intensity of BPDE-treated 293T-WT (n=87) and 293T-K164R (n=159) cells represented by box plots. Statistical analysis as Figure 2Aii. **** P <0.0001.

B. (i) Representative images of N=2 independent experiments. BPDE-treated (0.5 μM) U2OS sgPolK cells (Polκ -/-) and transfected with GFP-tagged PolK (+Polκ WT), GFP-tagged PolK UBZ mutant (+Polκ UBZ) or GFP-tagged PolK CD mutant (+Polκ CD) cells. Polκ expression in green, and EBndG in nucleus and nucleolar enrichment in red. Full image in Figure S6A. Scale bar = 10 μm.

(ii). Quantification of nuclear EBndG intensity of BPDE-treated U2OS sgPolK cells (Polκ -/-, n=206) and transfected with GFP-tagged PolK (+Polκ WT, n=220), GFP-tagged PolK UBZ mutant (+Polκ UBZ, n=197or GFP-tagged PolK CD mutant (+Polκ CD, n=207) cells represented by box plots. Statistical analysis as Figure 4Eii. **** P <0.0001, * P <0.0139.

Figure 7: Inhibition of PARylation by PARP1 inhibitor (olaparib) reduced recruitment of RNF2 and decreased the activity of Polκ

A. Representative images from *N*=2 independent experiments. Cells either treated with DMSO (control) or 10 μM Olaparib (for 3 days) (PARP1 PARylation inhibitor) were incubated with 0 or 2 μM BPDE. EBndG (red), PARP1 (gray), Polκ (green) and DAPI (blue). Full image in Figure S7A.

B. (i) Similar experiment as 7A, immunofluorescence with Polκ (green), RNF2 (gray), DAPI (blue) and EBndG (red). Full image in Figure S7B. Scale bars = 10 μm.

Quantification of 7B, total nuclear intensity of EBndG **(ii)**, Polκ **(iii)** and number of nuclear RNF2 foci **(iv)** in cells treated with olaparib and 0 μM BPDE (n=40) compared to BPDE-treated (2 μM) cells that were earlier incubated with either DMSO (n=125) or olaparib (n=153). Statistical analysis as Figure 4Eii. **** P <0.0001, *** P = 0.0002, ** P = 0.0064 .

D. Western blot analysis of Polκ expression in BPDE-treated with or without olaparib. Quantification of Polκ bands after normalization with GAPDH, FC compared to control (no olaparib treated) cells. The full blots are shown in Figure S10C.

Figure 8: The activity of Polκ in the nucleolus is associated with peripheral accumulation of Polycomb Protein, Ring Finger Protein 2 (RNF2)

A. (i) Representative images from *N*= 2 independent experiments with siScrambled or siRNF2 transfected cells. Immunofluorescence with Polκ (green) and RNF2 (gray). DAPI shown in blue and EBndG in red. Scale bar = 10 μm.

Quantification of 8A, total nuclear intensity of Polκ **(ii)**, EBndG **(iii)** and RNF2 **(iv)** in cells transfected with siSc or siRNF2. siRNF2 cells without BPDE-treatment (n=188), compared to 2μM BPDE treated siRNF2 (n=184) and siScrambled (n=168) cells. Statistical analysis as Figure 4Eii. **** P <0.0001, * P = 0.0408

B. Western blot analysis of Polκ and NPM1expression in U2OS cells treated with 0 or 2 μM BPDE. Vinculin as loading control. Low and high exposure of the western blots in Figure S10B.

C. Relative expression of POLK transcript in siSc and siPOLK transfected cells, after treatment with 0 and 2 μM BPDE. GAPDH mRNA as internal control. Calculated with the comparative CT method (mean ± SEM). All comparisons are relative to siSc 0 μM BPDE.

Figure 9: Polκ participates in recovering from nucleolar stress after BPDE damage

A. Quantification of nuclear γH2AX intensity in cells transfected with siSc or siPOLK after treatment with 0 and 2 μM BPDE. [siSc, BPDE 0 μM (n=136)], [siSc, BPDE 2 μM (n=96)], [siPOLK, BPDE 0 μM (n=259)], [siPOLK, BPDE 2 μM (n=141)]. Statistical analysis as described in Figure 2Aii. **** P <0.0001. Image of the cells in Figure S9A.

B. Relative expression of 47S pre-rRNA transcript in siSc and siPOLK transfected cells, after treatment with 0 and 2 μM BPDE. GAPDH mRNA as internal control. Calculated with the comparative CT method (mean ± SEM), three technical replicates from *N*=2. All comparisons are relative to siSc 0 μM BPDE.

C. (i) Representative images of EU incorporation (red) in nascent RNA in cells transfected with siScrambled or siPOLK. Polκ expression (green) and DAPI (blue). Full images in Figure S9B.

(ii) Quantification of these cells (n=25-40) treated with 0, 0.1, 0.5 μM BPDE. Statistical analysis as described in Figure 2Aii. **** P <0.0001, *** P = 0.0002.

D. (i) Representative images of BPDE-treated (0.5 μM) U2OS sgPolK cells (Polκ -/-) and transfected with GFP-tagged PolK (+Polκ WT). Polκ expression (green), nucleolar EU incorporation (red, shown by an arrow) and DAPI (blue). Full images in Figure S9C.

(ii) Quantification of the nuclear EU intensity of U2OS Polκ -/- (n=35) and +Polκ WT (n=86). Statistical analysis as Figure 2Aii. **** P <0.0001.

E. Experimental design to identify the role of Polκ in BPDE-induced nucleolar stress recovery after 36 hours.

F. Representative images of cells transfected with siScrambled or siPOLK, treated with BPDE (0.5 or 2 μM) and fixed for immunofluorescence (t=2 h) or recovered after t=36 h. Immunofluorescence showing Polκ (green), EBndG (red), NPM1 (gray) and DAPI (blue).

Full images in Figure S9D.

G. Representative images of cells transfected with siScrambled or siPOLK, treated with BPDE (0.5) and fixed for immunofluorescence (t=2 h) or recovered after t=36 h. Immunofluorescence showing UBF1 (green) and DAPI (gray). Full images in Figure S9E. All scale bars 10 μm.

Figure 10: Working model on the role of Polκ in recovering from nucleolar stress after BPDE damage

Upon exposure to DNA damaging agents (BPDE, cisplatin, MMC) or RNAPI inhibitor (actinomycin D), DNA damages are formed on genomic DNA including rDNA. Cells undergo nucleolar stress, with inhibition of rDNA transcription, nucleolar protein NPM1 release to nucleoplasm and nucleolar cap formation for rDNA repair. The DNA damage signals monoubiquitination (Ub) of PCNA, as well as recruitment of PARP1 that creates PARylation on chromatin at the damaged sites. PARylation initiates PRC1 proteins (including RNF2) to form polycomb bodies near NADs. In wild type cells (left), PCNA Ub and PARylation with PRC1 body formation regulates Polκ protein recruitment to the damaged sites, stabilization and therefore higher Polκ activity in the nucleolus, evident by enrichment of EBndG in the nucleolus. Presence of Polκ facilitates cells to gradually recover from rDNA damage-induced nucleolar stress. However, in Polκ-depleted cells (right), the nucleolar stress is retained, and cells fail to recover from nucleolar stress.

Acknowledgements

We would like to thank G. Lucian Moldovan for critically reading the manuscript, providing olaparib, the PARP1 and vinculin antibody, and the 293T-K164R cells; and Zhonghua Gao for providing the RNF2 antibody, H2AK119Ub antibody, siRNF2 and for expertise on Polycomb complex proteins. Benzo[a]pyrene diol epoxide was provided by the Organic Synthesis Core of the Penn State Cancer Institute. We would like to thank Peter Tonzi for technical assistance with sgU2OS sgPolK cells. This work was supported by NIH grants R01ES021762 (TES), GM139610 and ES031658 (T.T.H.).

Author contributions

The project was conceived by TES and S.P. EBndG reagent was designed and generated by T.S. All experiments were designed and performed by S.P. Cell viability assay, western blots and cell culture were maintained by A.R. Proteomics experimental guidance were provided by D.P and P.C. Mass spectrometry experiments were performed and data analyzed by P.C. Super-resolution confocal microscopy was performed under guidance of A.P. The cell profiler pipelines were generated by A.P. Polk knockout cells were provided by T.T.H. The paper was written by S.P and T.S with contributions from other authors.

(1) Vaisman, A.; Woodgate, R. Translesion DNA Polymerases in Eukaryotes: What Makes Them Tick? *Crit Rev Biochem Mol Biol* **2017**, *52* (3), 274–303. https://doi.org/10.1080/10409238.2017.1291576.

(2) Dipple, A. DNA Adducts of Chemical Carcinogens. *Carcinogenesis* **1995**, *16* (3), 437–441. https://doi.org/10.1093/carcin/16.3.437.

(3) Ohmori, H.; Ohashi, E.; Ogi, T. Mammalian Pol Kappa: Regulation of Its Expression and Lesion Substrates. *Adv Protein Chem* **2004**, *69*, 265–278. https://doi.org/10.1016/S0065-3233(04)69009-7.

(4) Avkin, S.; Goldsmith, M.; Velasco-Miguel, S.; Geacintov, N.; Friedberg, E. C.; Livneh, Z. Quantitative Analysis of Translesion DNA Synthesis across a Benzo[a]Pyrene-Guanine Adduct in Mammalian Cells: THE ROLE OF DNA POLYMERASE κ *. *Journal of Biological Chemistry* **2004**, *279* (51), 53298–53305. https://doi.org/10.1074/jbc.M409155200.

(5) Shachar, S.; Ziv, O.; Avkin, S.; Adar, S.; Wittschieben, J.; Reißner, T.; Chaney, S.; Friedberg, E. C.; Wang, Z.; Carell, T.; Geacintov, N.; Livneh, Z. Two-Polymerase Mechanisms Dictate Error-Free and Error-Prone Translesion DNA Synthesis in Mammals. *EMBO J* **2009**, *28* (4), 383–393. https://doi.org/10.1038/emboj.2008.281.

(6) Jha, V.; Ling, H. Structural Basis for Human DNA Polymerase Kappa to Bypass Cisplatin Intrastrand Cross-Link (Pt-GG) Lesion as an Efficient and Accurate Extender. *J Mol Biol* **2018**, *430* (11), 1577–1589. https://doi.org/10.1016/j.jmb.2018.04.023.

(7) Stern, H. R.; Sefcikova, J.; Chaparro, V. E.; Beuning, P. J. Mammalian DNA Polymerase Kappa Activity and Specificity. **2019**, 20.

(8) Bi, X.; Barkley, L. R.; Slater, D. M.; Tateishi, S.; Yamaizumi, M.; Ohmori, H.; Vaziri, C. Rad18 Regulates DNA Polymerase Kappa and Is Required for Recovery from S-Phase Checkpoint-Mediated Arrest. *Mol Cell Biol* **2006**, *26* (9), 3527–3540. https://doi.org/10.1128/MCB.26.9.3527-3540.2006.

(9) Ogi, T.; Lehmann, A. R. The Y-Family DNA Polymerase κ (Pol κ) Functions in Mammalian Nucleotide-Excision Repair. *Nat Cell Biol* **2006**, *8* (6), 640–642. https://doi.org/10.1038/ncb1417.

(10) Minko, I. G.; Yamanaka, K.; Kozekov, I. D.; Kozekova, A.; Indiani, C.; O'Donnell, M. E.; Jiang, Q.; Goodman, M. F.; Rizzo, C. J.; Lloyd, R. S. Replication Bypass of the Acrolein-Mediated Deoxyguanine DNA-Peptide Cross-Links by DNA Polymerases of the DinB Family. *Chem Res Toxicol* **2008**, *21* (10), 1983–1990. https://doi.org/10.1021/tx800174a.

(11) Williams, H. L.; Gottesman, M. E.; Gautier, J. Replication-Independent Repair of DNA Interstrand Crosslinks. *Mol Cell* **2012**, *47* (1), 140–147. https://doi.org/10.1016/j.molcel.2012.05.001.

(12) Bétous, R.; Pillaire, M.-J.; Pierini, L.; van der Laan, S.; Recolin, B.; Ohl-Séguy, E.; Guo, C.; Niimi, N.; Grúz, P.; Nohmi, T.; Friedberg, E.; Cazaux, C.; Maiorano, D.; Hoffmann, J.-S. DNA Polymerase κ-Dependent DNA Synthesis at Stalled Replication Forks Is Important for CHK1 Activation. *The EMBO Journal* **2013**, *32* (15), 2172–2185. https://doi.org/10.1038/emboj.2013.148.

(13) Baptiste, B. A.; Eckert, K. A. DNA Polymerase Kappa Microsatellite Synthesis: Two Distinct Mechanisms of Slippage-Mediated Errors. *Environmental and Molecular Mutagenesis* **2012**, *53* (9), 787–796. https://doi.org/10.1002/em.21721.

(14) Walsh, E.; Wang, X.; Lee, M. Y.; Eckert, K. A. Mechanism of Replicative DNA Polymerase Delta Pausing and a Potential Role for DNA Polymerase Kappa in Common Fragile Site Replication. *J Mol Biol* **2013**, *425* (2), 232–243. https://doi.org/10.1016/j.jmb.2012.11.016.

(15) Prakasha Gowda, A. S.; Lee, M.; Spratt, T. E. N2-Substituted 2′-Deoxyguanosine Triphosphate Derivatives, Selective Substrates for Human DNA Polymerase κ. *Angew Chem Int Ed Engl* **2017**, *56* (10), 2628–2631. https://doi.org/10.1002/anie.201611607.

(16) Rudra, D.; Warner, J. R. What Better Measure than Ribosome Synthesis? *Genes Dev* **2004**, *18* (20), 2431–2436. https://doi.org/10.1101/gad.1256704.

(17) Gaillard, H.; García-Muse, T.; Aguilera, A. Replication Stress and Cancer. *Nat Rev Cancer* **2015**, *15* (5), 276–289. https://doi.org/10.1038/nrc3916.

(18) Gottipati, P.; Cassel, T. N.; Savolainen, L.; Helleday, T. Transcription-Associated Recombination Is Dependent on Replication in Mammalian Cells. *Mol Cell Biol* **2008**, *28* (1), 154–164. https://doi.org/10.1128/MCB.00816-07.

(19) Aguilera, A.; Gómez-González, B. Genome Instability: A Mechanistic View of Its Causes and Consequences. *Nat Rev Genet* **2008**, *9* (3), 204–217. https://doi.org/10.1038/nrg2268.

(20) Li, X.; Manley, J. L. Cotranscriptional Processes and Their Influence on Genome Stability. *Genes Dev.* **2006**, *20* (14), 1838–1847. https://doi.org/10.1101/gad.1438306.

(21) Gan, W.; Guan, Z.; Liu, J.; Gui, T.; Shen, K.; Manley, J. L.; Li, X. R-Loop-Mediated Genomic Instability Is Caused by Impairment of Replication Fork Progression. *Genes Dev.* **2011**, *25* (19), 2041–2056. https://doi.org/10.1101/gad.17010011.

(22) Lindström, M. S.; Jurada, D.; Bursac, S.; Orsolic, I.; Bartek, J.; Volarevic, S. Nucleolus as an Emerging Hub in Maintenance of Genome Stability and Cancer Pathogenesis. *Oncogene* **2018**, *37* (18), 2351–2366. https://doi.org/10.1038/s41388-017-0121-z.

(23) Pederson, T. The Nucleolus. *Cold Spring Harb Perspect Biol* **2011**, *3* (3), a000638. https://doi.org/10.1101/cshperspect.a000638.

(24) Farley, K. I.; Surovtseva, Y.; Merkel, J.; Baserga, S. J. Determinants of Mammalian Nucleolar Architecture. *Chromosoma* **2015**, *124* (3), 323–331. https://doi.org/10.1007/s00412-015-0507-z.

(25) Kruhlak, M.; Crouch, E. E.; Orlov, M.; Montaño, C.; Gorski, S. A.; Nussenzweig, A.; Misteli, T.; Phair, R. D.; Casellas, R. The ATM Repair Pathway Inhibits RNA Polymerase I Transcription in Response to Chromosome Breaks. *Nature* **2007**, *447* (7145), 730–734. https://doi.org/10.1038/nature05842.

(26) Harding, S. M.; Boiarsky, J. A.; Greenberg, R. A. ATM Dependent Silencing Links Nucleolar Chromatin Reorganization to DNA Damage Recognition. *Cell Rep* **2015**, *13* (2), 251–259. https://doi.org/10.1016/j.celrep.2015.08.085.

(27) van Sluis, M.; McStay, B. A Localized Nucleolar DNA Damage Response Facilitates Recruitment of the Homology-Directed Repair Machinery Independent of Cell Cycle Stage. *Genes Dev* **2015**, *29* (11), 1151–1163. https://doi.org/10.1101/gad.260703.115.

(28) van Sluis, M.; McStay, B. Nucleolar Reorganization in Response to RDNA Damage. *Curr Opin Cell Biol* **2017**, *46*, 81–86. https://doi.org/10.1016/j.ceb.2017.03.004.

(29) Wang, H.; Chen, T.; Weng, C.; Yang, C.; Tang, M. Acrolein Preferentially Damages Nucleolus Eliciting Ribosomal Stress and Apoptosis in Human Cancer Cells. *Oncotarget* **2016**, *7* (49), 80450–80464. https://doi.org/10.18632/oncotarget.12608.

(30) Korsholm, L. M.; Gál, Z.; Nieto, B.; Quevedo, O.; Boukoura, S.; Lund, C. C.; Larsen, D. H. Recent Advances in the Nucleolar Responses to DNA Double-Strand Breaks. *Nucleic Acids Res* **2020**, *48* (17), 9449–9461. https://doi.org/10.1093/nar/gkaa713.

(31) Sutton, E. C.; DeRose, V. J. Early Nucleolar Responses Differentiate Mechanisms of Cell Death Induced by Oxaliplatin and Cisplatin. *J Biol Chem* **2021**, *296*, 100633. https://doi.org/10.1016/j.jbc.2021.100633.

(32) Yang, Y.; Hu, J.; Selby, C. P.; Li, W.; Yimit, A.; Jiang, Y.; Sancar, A. Single-Nucleotide Resolution Analysis of Nucleotide Excision Repair of Ribosomal DNA in Humans and Mice. *Journal of Biological Chemistry* **2019**, *294* (1), 210–217. https://doi.org/10.1074/jbc.RA118.006121.

(33) Ahmad, Y.; Boisvert, F.-M.; Gregor, P.; Cobley, A.; Lamond, A. I. NOPdb: Nucleolar Proteome Database--2008 Update. *Nucleic Acids Res* **2009**, *37* (Database issue), D181-184. https://doi.org/10.1093/nar/gkn804.

(34) Ogawa, L. M.; Baserga, S. J. Crosstalk between the Nucleolus and the DNA Damage Response. *Mol Biosyst* **2017**, *13* (3), 443–455. https://doi.org/10.1039/c6mb00740f.

(35) Moore, H. M.; Bai, B.; Boisvert, F.-M.; Latonen, L.; Rantanen, V.; Simpson, J. C.; Pepperkok, R.; Lamond, A. I.; Laiho, M. Quantitative Proteomics and Dynamic Imaging of the Nucleolus Reveal Distinct Responses to UV and Ionizing Radiation. *Mol Cell Proteomics* **2011**, *10* (10), M111.009241. https://doi.org/10.1074/mcp.M111.009241.

(36) Andersen, J. S.; Lam, Y. W.; Leung, A. K. L.; Ong, S.-E.; Lyon, C. E.; Lamond, A. I.; Mann, M. Nucleolar Proteome Dynamics. *Nature* **2005**, *433* (7021), 77–83. https://doi.org/10.1038/nature03207.

(37) Yung, T. M. C.; Sato, S.; Satoh, M. S. Poly(ADP-Ribosyl)Ation as a DNA Damage-Induced Post-Translational Modification Regulating Poly(ADP-Ribose) Polymerase-1-Topoisomerase I Interaction. *J Biol Chem* **2004**, *279* (38), 39686–39696. https://doi.org/10.1074/jbc.M402729200.

(38) Rancourt, A.; Satoh, M. S. Delocalization of Nucleolar Poly(ADP-Ribose) Polymerase-1 to the Nucleoplasm and Its Novel Link to Cellular Sensitivity to DNA Damage. *DNA Repair (Amst)* **2009**, *8* (3), 286–297. https://doi.org/10.1016/j.dnarep.2008.11.018.

(39) Rubbi, C. P.; Milner, J. Disruption of the Nucleolus Mediates Stabilization of P53 in Response to DNA Damage and Other Stresses. *EMBO J* **2003**, *22* (22), 6068–6077. https://doi.org/10.1093/emboj/cdg579.

(40) Xuan, J.; Gitareja, K.; Brajanovski, N.; Sanij, E. Harnessing the Nucleolar DNA Damage Response in Cancer Therapy. *Genes (Basel)* **2021**, *12* (8), 1156. https://doi.org/10.3390/genes12081156.

(41) Boulon, S.; Westman, B. J.; Hutten, S.; Boisvert, F.-M.; Lamond, A. I. The Nucleolus under Stress. *Mol Cell* **2010**, *40* (2), 216–227. https://doi.org/10.1016/j.molcel.2010.09.024.

(42) Ziv, O.; Zeisel, A.; Mirlas-Neisberg, N.; Swain, U.; Nevo, R.; Ben-Chetrit, N.; Martelli, M. P.; Rossi, R.; Schiesser, S.; Canman, C. E.; Carell, T.; Geacintov, N. E.; Falini, B.; Domany, E.; Livneh, Z. Identification of Novel DNA-Damage Tolerance Genes Reveals Regulation of

Translesion DNA Synthesis by Nucleophosmin. *Nat Commun* **2014**, *5* (1), 5437. https://doi.org/10.1038/ncomms6437.

(43) Leung, K. H. T.; El Hassan, M. A.; Bremner, R. A Rapid and Efficient Method to Purify Proteins at Replication Forks under Native Conditions. *BioTechniques* **2013**, *55* (4), 204–206. https://doi.org/10.2144/000114089.

(44) Alabert, C.; Bukowski-Wills, J. C.; Lee, S. B.; Kustatscher, G.; Nakamura, K.; De Lima Alves, F.; Menard, P.; Mejlvang, J.; Rappsilber, J.; Groth, A. Nascent Chromatin Capture Proteomics Determines Chromatin Dynamics during DNA Replication and Identifies Unknown Fork Components. *Nature Cell Biology* **2014**, *16* (3), 281–291. https://doi.org/10.1038/ncb2918.

(45) Dungrawala, H.; Rose, K. L.; Bhat, K. P.; Mohni, K. N.; Glick, G. G.; Couch, F. B.; Cortez, D. The Replication Checkpoint Prevents Two Types of Fork Collapse without Regulating Replisome Stability. *Mol Cell* **2015**, *59* (6), 998–1010. https://doi.org/10.1016/j.molcel.2015.07.030.

(46) Wessel, S. R.; Mohni, K. N.; Luzwick, J. W.; Dungrawala, H.; Cortez, D. Functional Analysis of the Replication Fork Proteome Identifies BET Proteins as PCNA Regulators. *Cell Rep* **2019**, *28* (13), 3497-3509.e4. https://doi.org/10.1016/j.celrep.2019.08.051.

(47) Romagnolo, D.; Jeffy, B.; Samuelson, D.; Payne, C. Microarray Expression Profiles in Breast Cancer MCF-7 Cells Following Exposure to Benzo[a]Pyrene and Its Diol Epoxide. *Nat Genet* **2001**, *27* (4), 83–83. https://doi.org/10.1038/87272.

(48) Bryant, C. J.; McCool, M. A.; Abriola, L.; Surovtseva, Y. V.; Baserga, S. J. A High-Throughput Assay for Directly Monitoring Nucleolar RRNA Biogenesis. *Open Biol* **2022**, *12* (1), 210305. https://doi.org/10.1098/rsob.210305.

(49) Zhuo, M.; Gorgun, M. F.; Englander, E. W. Translesion Synthesis DNA Polymerase Kappa Is Indispensable for DNA Repair Synthesis in Cisplatin Exposed Dorsal Root Ganglion Neurons. *Mol Neurobiol* **2018**, *55* (3), 2506–2515. https://doi.org/10.1007/s12035-017-0507-5.

(50) Spanjaard, A.; Shah, R.; de Groot, D.; Buoninfante, O. A.; Morris, B.; Lieftink, C.; Pritchard, C.; Zürcher, L. M.; Ormel, S.; Catsman, J. J. I.; de Korte-Grimmerink, R.; Siteur, B.; Proost, N.; Boadum, T.; van de Ven, M.; Song, J.-Y.; Kreft, M.; van den Berk, P. C. M.; Beijersbergen, R. L.; Jacobs, H. Division of Labor within the DNA Damage Tolerance System Reveals Non-Epistatic and Clinically Actionable Targets for Precision Cancer Medicine. *Nucleic Acids Research* **2022**, *50* (13), 7420–7435. https://doi.org/10.1093/nar/gkac545.

(51) Kanemaru, Y.; Suzuki, T.; Sassa, A.; Matsumoto, K.; Adachi, N.; Honma, M.; Numazawa, S.; Nohmi, T. DNA Polymerase Kappa Protects Human Cells against MMC-Induced Genotoxicity through Error-Free Translesion DNA Synthesis. *Genes Environ* **2017**, *39*, 6. https://doi.org/10.1186/s41021-016-0067-3.

(52) Takeiri, A.; Wada, N. A.; Motoyama, S.; Matsuzaki, K.; Tateishi, H.; Matsumoto, K.; Niimi, N.; Sassa, A.; Grúz, P.; Masumura, K.; Yamada, M.; Mishima, M.; Jishage, K.; Nohmi, T. In Vivo Evidence That DNA Polymerase Kappa Is Responsible for Error-Free Bypass across DNA Cross-Links Induced by Mitomycin C. *DNA Repair* **2014**, *24*, 113–121. https://doi.org/10.1016/j.dnarep.2014.09.002.

(53) Schoefl, G. I. The Effect of Actinomycin D on the Fine Structure of the Nucleolus. *Journal of Ultrastructure Research* **1964**, *10* (3), 224–243. https://doi.org/10.1016/S0022-5320(64)80007-1.

(54) Tonzi, P.; Yin, Y.; Lee, C. W. T.; Rothenberg, E.; Huang, T. T. Translesion Polymerase Kappa-Dependent DNA Synthesis Underlies Replication Fork Recovery. *eLife 7*, e41426. https://doi.org/10.7554/eLife.41426.

(55) Hoege, C.; Pfander, B.; Moldovan, G.-L.; Pyrowolakis, G.; Jentsch, S. RAD6-Dependent DNA Repair Is Linked to Modification of PCNA by Ubiquitin and SUMO. *Nature* **2002**, *419* (6903), 135–141. https://doi.org/10.1038/nature00991.

(56) Lehmann, A. R.; Niimi, A.; Ogi, T.; Brown, S.; Sabbioneda, S.; Wing, J. F.; Kannouche, P. L.; Green, C. M. Translesion Synthesis: Y-Family Polymerases and the Polymerase Switch. *DNA Repair (Amst)* **2007**, *6* (7), 891–899. https://doi.org/10.1016/j.dnarep.2007.02.003.

(57) Ghosal, G.; Chen, J. DNA Damage Tolerance: A Double-Edged Sword Guarding the Genome. *Translational Cancer Research* **2013**, *2* (3). https://doi.org/10.3978/j.issn.2218-676X.2013.04.01.

(58) Choe, K. N.; Moldovan, G.-L. Forging Ahead through Darkness: PCNA, Still the Principal Conductor at the Replication Fork. *Mol Cell* **2017**, *65* (3), 380–392. https://doi.org/10.1016/j.molcel.2016.12.020.

(59) Jones, M. J.; Colnaghi, L.; Huang, T. T. Dysregulation of DNA Polymerase κ Recruitment to Replication Forks Results in Genomic Instability. *The EMBO Journal* **2012**, *31* (4), 908–918. https://doi.org/10.1038/emboj.2011.457.

(60) Thakar, T.; Leung, W.; Nicolae, C. M.; Clements, K. E.; Shen, B.; Bielinsky, A.-K.; Moldovan, G.-L. Ubiquitinated-PCNA Protects Replication Forks from DNA2-Mediated Degradation by Regulating Okazaki Fragment Maturation and Chromatin Assembly. *Nat Commun* **2020**, *11* (1), 2147. https://doi.org/10.1038/s41467-020-16096-w.

(61) Kannouche, P. L.; Wing, J.; Lehmann, A. R. Interaction of Human DNA Polymerase Eta with Monoubiquitinated PCNA: A Possible Mechanism for the Polymerase Switch in Response to DNA Damage. *Mol Cell* **2004**, *14* (4), 491–500. https://doi.org/10.1016/s1097-2765(04)00259-x.

(62) Bienko, M.; Green, C. M.; Crosetto, N.; Rudolf, F.; Zapart, G.; Coull, B.; Kannouche, P.; Wider, G.; Peter, M.; Lehmann, A. R.; Hofmann, K.; Dikic, I. Ubiquitin-Binding Domains in Y-Family Polymerases Regulate Translesion Synthesis. *Science* **2005**, *310* (5755), 1821–1824. https://doi.org/10.1126/science.1120615.

(63) Ohmori, H.; Hanafusa, T.; Ohashi, E.; Vaziri, C. Separate Roles of Structured and Unstructured Regions of Y-Family DNA Polymerases. In *Advances in Protein Chemistry and Structural Biology*; McPherson, A., Ed.; Advances in Protein Chemistry and Structural Biology; Academic Press, 2009; Vol. 78, pp 99–146. https://doi.org/10.1016/S1876-1623(08)78004-0.

(64) Gerlach, V. L.; Feaver, W. J.; Fischhaber, P. L.; Friedberg, E. C. Purification and Characterization of Polκ, a DNA Polymerase Encoded by the Human DINB1 Gene *. *Journal of Biological Chemistry* **2001**, *276* (1), 92–98. https://doi.org/10.1074/jbc.M004413200.

(65) Lancey, C.; Tehseen, M.; Bakshi, S.; Percival, M.; Takahashi, M.; Sobhy, M. A.; Raducanu, V. S.; Blair, K.; Muskett, F. W.; Ragan, T. J.; Crehuet, R.; Hamdan, S. M.; De

Biasio, A. Cryo-EM Structure of Human Pol κ Bound to DNA and Mono-Ubiquitylated PCNA. *Nat Commun* **2021**, *12* (1), 6095. https://doi.org/10.1038/s41467-021-26251-6.

(66) Lone, S.; Townson, S. A.; Uljon, S. N.; Johnson, R. E.; Brahma, A.; Nair, D. T.; Prakash, S.; Prakash, L.; Aggarwal, A. K. Human DNA Polymerase κ Encircles DNA: Implications for Mismatch Extension and Lesion Bypass. *Molecular Cell* **2007**, *25* (4), 601–614. https://doi.org/10.1016/j.molcel.2007.01.018.

(67) Gagné, J.-P.; Isabelle, M.; Lo, K. S.; Bourassa, S.; Hendzel, M. J.; Dawson, V. L.; Dawson, T. M.; Poirier, G. G. Proteome-Wide Identification of Poly(ADP-Ribose) Binding Proteins and Poly(ADP-Ribose)-Associated Protein Complexes. *Nucleic Acids Res* **2008**, *36* (22), 6959–6976. https://doi.org/10.1093/nar/gkn771.

(68) Isabelle, M.; Moreel, X.; Gagné, J.-P.; Rouleau, M.; Ethier, C.; Gagné, P.; Hendzel, M. J.; Poirier, G. G. Investigation of PARP-1, PARP-2, and PARG Interactomes by Affinity-Purification Mass Spectrometry. *Proteome Sci* **2010**, *8*, 22. https://doi.org/10.1186/1477-5956-8-22.

(69) Jungmichel, S.; Rosenthal, F.; Altmeyer, M.; Lukas, J.; Hottiger, M. O.; Nielsen, M. L. Proteome-Wide Identification of Poly(ADP-Ribosyl)Ation Targets in Different Genotoxic Stress Responses. *Mol Cell* **2013**, *52* (2), 272–285. https://doi.org/10.1016/j.molcel.2013.08.026.

(70) Krietsch, J.; Rouleau, M.; Pic, É.; Ethier, C.; Dawson, T. M.; Dawson, V. L.; Masson, J.-Y.; Poirier, G. G.; Gagné, J.-P. Reprogramming Cellular Events by Poly(ADP-Ribose)-Binding Proteins. *Mol Aspects Med* **2013**, *34* (6), 1066–1087. https://doi.org/10.1016/j.mam.2012.12.005.

(71) Fischer, J. M. F.; Zubel, T.; Jander, K.; Fix, J.; Trussina, I. R. E. A.; Gebhard, D.; Bergemann, J.; Bürkle, A.; Mangerich, A. PARP1 Protects from Benzo[a]Pyrene Diol Epoxide-Induced Replication Stress and Mutagenicity. *Arch Toxicol* **2018**, *92* (3), 1323–1340. https://doi.org/10.1007/s00204-017-2115-6.

(72) Rona, G.; Roberti, D.; Yin, Y.; Pagan, J. K.; Homer, H.; Sassani, E.; Zeke, A.; Busino, L.; Rothenberg, E.; Pagano, M. PARP1-Dependent Recruitment of the FBXL10-RNF68-RNF2 Ubiquitin Ligase to Sites of DNA Damage Controls H2A.Z Loading. *eLife* **2018**, *7*, e38771. https://doi.org/10.7554/eLife.38771.

(73) Pirrotta, V.; Li, H.-B. A View of Nuclear Polycomb Bodies. *Curr Opin Genet Dev* **2012**, *22* (2), 101–109. https://doi.org/10.1016/j.gde.2011.11.004.

(74) Bizhanova, A.; Kaufman, P. D. Close to the Edge: Heterochromatin at the Nucleolar and Nuclear Peripheries. *Biochim Biophys Acta Gene Regul Mech* **2021**, *1864* (1), 194666. https://doi.org/10.1016/j.bbagrm.2020.194666.

(75) Tamburri, S.; Lavarone, E.; Fernández-Pérez, D.; Conway, E.; Zanotti, M.; Manganaro, D.; Pasini, D. Histone H2AK119 Mono-Ubiquitination Is Essential for Polycomb-Mediated Transcriptional Repression. *Mol Cell* **2020**, *77* (4), 840-856.e5. https://doi.org/10.1016/j.molcel.2019.11.021.

(76) Bi, X.; Slater, D. M.; Ohmori, H.; Vaziri, C. DNA Polymerase Kappa Is Specifically Required for Recovery from the Benzo[a]Pyrene-Dihydrodiol Epoxide (BPDE)-Induced S-Phase Checkpoint. *J Biol Chem* **2005**, *280* (23), 22343–22355. https://doi.org/10.1074/jbc.M501562200.

(77) Mattsson, A.; Jernström, B.; Cotgreave, I. A.; Bajak, E. H2AX Phosphorylation in A549 Cells Induced by the Bulky and Stable DNA Adducts of Benzo[a]Pyrene and Dibenzo[a,l]Pyrene Diol Epoxides. *Chem Biol Interact* **2009**, *177* (1), 40–47. https://doi.org/10.1016/j.cbi.2008.09.015.

(78) Lee, Y.-J.; Park, S.-J.; Ciccone, S. L. M.; Kim, C.-R.; Lee, S.-H. An in Vivo Analysis of MMC-Induced DNA Damage and Its Repair. *Carcinogenesis* **2006**, *27* (3), 446–453. https://doi.org/10.1093/carcin/bgi254.

(79) Lemaire, M. A.; Schwartz, A.; Rahmouni, A. R.; Leng, M. Interstrand Cross-Links Are Preferentially Formed at the d(GC) Sites in the Reaction between Cis-Diamminedichloroplatinum (II) and DNA. *Proc Natl Acad Sci U S A* **1991**, *88* (5), 1982–1985.

(80) Perry, R. P.; Kelley, D. E. Inhibition of RNA Synthesis by Actinomycin D: Characteristic Dose-Response of Different RNA Species. *J Cell Physiol* **1970**, *76* (2), 127–139. https://doi.org/10.1002/jcp.1040760202.

(81) Jordan, P.; Carmo-Fonseca, M. Cisplatin Inhibits Synthesis of Ribosomal RNA in Vivo. *Nucleic Acids Res* **1998**, *26* (12), 2831–2836.

(82) James, A.; Wang, Y.; Raje, H.; Rosby, R.; DiMario, P. Nucleolar Stress with and without P53. *Nucleus* **2014**, *5* (5), 402–426. https://doi.org/10.4161/nucl.32235.

(83) Snodgrass, R. G.; Collier, A. C.; Coon, A. E.; Pritsos, C. A. Mitomycin C Inhibits Ribosomal RNA. *J Biol Chem* **2010**, *285* (25), 19068–19075. https://doi.org/10.1074/jbc.M109.040477.

(84) Tubbs, A.; Nussenzweig, A. Endogenous DNA Damage as a Source of Genomic Instability in Cancer. *Cell* **2017**, *168* (4), 644–656. https://doi.org/10.1016/j.cell.2017.01.002.

(85) Zhou, H.; Wang, Y.; Wang, Q.; Li, L.; Hu, Y.; Wu, Y.; Gautam, M.; Li, L. R-Loops Mediate Transcription-Associated Formation of Human RDNA Secondary Constrictions. *J Cell Biochem* **2021**, *122* (10), 1517–1533. https://doi.org/10.1002/jcb.30074.

(86) Chan, Y. A.; Aristizabal, M. J.; Lu, P. Y. T.; Luo, Z.; Hamza, A.; Kobor, M. S.; Stirling, P. C.; Hieter, P. Genome-Wide Profiling of Yeast DNA:RNA Hybrid Prone Sites with DRIP-Chip. *PLOS Genetics* **2014**, *10* (4), e1004288. https://doi.org/10.1371/journal.pgen.1004288.

(87) Sollier, J.; Cimprich, K. A. Breaking Bad: R-Loops and Genome Integrity. *Trends Cell Biol* **2015**, *25* (9), 514–522. https://doi.org/10.1016/j.tcb.2015.05.003.

(88) Yang, X.; Liu, Q.-L.; Xu, W.; Zhang, Y.-C.; Yang, Y.; Ju, L.-F.; Chen, J.; Chen, Y.-S.; Li, K.; Ren, J.; Sun, Q.; Yang, Y.-G. M6A Promotes R-Loop Formation to Facilitate Transcription Termination. *Cell Res* **2019**, *29* (12), 1035–1038. https://doi.org/10.1038/s41422-019-0235-7.

(89) Abakir, A.; Giles, T. C.; Cristini, A.; Foster, J. M.; Dai, N.; Starczak, M.; Rubio-Roldan, A.; Li, M.; Eleftheriou, M.; Crutchley, J.; Flatt, L.; Young, L.; Gaffney, D. J.; Denning, C.; Dalhus, B.; Emes, R. D.; Gackowski, D.; Corrêa, I. R.; Garcia-Perez, J. L.; Klungland, A.; Gromak, N.; Ruzov, A. N6-Methyladenosine Regulates the Stability of RNA:DNA Hybrids in Human Cells. *Nat Genet* **2020**, *52* (1), 48–55. https://doi.org/10.1038/s41588-019-0549-x.

(90) Zhang, C.; Chen, L.; Peng, D.; Jiang, A.; He, Y.; Zeng, Y.; Xie, C.; Zhou, H.; Luo, X.; Liu, H.; Chen, L.; Ren, J.; Wang, W.; Zhao, Y. METTL3 and N6-Methyladenosine Promote Homologous Recombination-Mediated Repair of DSBs by Modulating DNA-RNA Hybrid Accumulation. *Mol Cell* **2020**, *79* (3), 425-442.e7. https://doi.org/10.1016/j.molcel.2020.06.017.

(91) Xiang, Y.; Laurent, B.; Hsu, C.-H.; Nachtergaele, S.; Lu, Z.; Sheng, W.; Xu, C.; Chen, H.; Ouyang, J.; Wang, S.; Ling, D.; Hsu, P.-H.; Zou, L.; Jambhekar, A.; He, C.; Shi, Y. RNA M6A Methylation Regulates the Ultraviolet-Induced DNA Damage Response. *Nature* **2017**, *543* (7646), 573–576. https://doi.org/10.1038/nature21671.

(92) Tornaletti, S. Transcription Arrest at DNA Damage Sites. *Mutation Research/Fundamental and Molecular Mechanisms of Mutagenesis* **2005**, *577* (1), 131–145. https://doi.org/10.1016/j.mrfmmm.2005.03.014.

(93) Geijer, M. E.; Marteijn, J. A. What Happens at the Lesion Does Not Stay at the Lesion: Transcription-Coupled Nucleotide Excision Repair and the Effects of DNA Damage on Transcription in Cis and Trans. *DNA Repair (Amst)* **2018**, *71*, 56–68. https://doi.org/10.1016/j.dnarep.2018.08.007.

(94) Steurer, B.; Janssens, R. C.; Geijer, M. E.; Aprile-Garcia, F.; Geverts, B.; Theil, A. F.; Hummel, B.; van Royen, M. E.; Evers, B.; Bernards, R.; Houtsmuller, A. B.; Sawarkar, R.; Marteijn, J. DNA Damage-Induced Transcription Stress Triggers the Genome-Wide Degradation of Promoter-Bound Pol II. *Nat Commun* **2022**, *13* (1), 3624. https://doi.org/10.1038/s41467-022-31329-w.

(95) Guo, C.; Tang, T.-S.; Bienko, M.; Dikic, I.; Friedberg, E. C. Requirements for the Interaction of Mouse Polkappa with Ubiquitin and Its Biological Significance. *J Biol Chem* **2008**, *283* (8), 4658–4664. https://doi.org/10.1074/jbc.M709275200.

(96) Stenström, L.; Mahdessian, D.; Gnann, C.; Cesnik, A. J.; Ouyang, W.; Leonetti, M. D.; Uhlén, M.; Cuylen-Haering, S.; Thul, P. J.; Lundberg, E. Mapping the Nucleolar Proteome

Reveals a Spatiotemporal Organization Related to Intrinsic Protein Disorder. *Molecular Systems Biology* **2020**, *16* (8), e9469. https://doi.org/10.15252/msb.20209469.

(97) Mashimo, M.; Onishi, M.; Uno, A.; Tanimichi, A.; Nobeyama, A.; Mori, M.; Yamada, S.; Negi, S.; Bu, X.; Kato, J.; Moss, J.; Sanada, N.; Kizu, R.; Fujii, T. The 89-KDa PARP1 Cleavage Fragment Serves as a Cytoplasmic PAR Carrier to Induce AIF-Mediated Apoptosis. *J Biol Chem* **2021**, *296*, 100046. https://doi.org/10.1074/jbc.RA120.014479.

(98) Wiest, N. E.; Tomkinson, A. E. Chapter One - Optimization of Native and Formaldehyde IPOND Techniques for Use in Suspension Cells. In *Methods in Enzymology*; Eichman, B. F., Ed.; DNA Repair Enzymes: Cell, Molecular, and Chemical Biology; Academic Press, 2017; Vol. 591, pp 1–32. https://doi.org/10.1016/bs.mie.2017.03.001.

(99) Carpenter, A. E.; Jones, T. R.; Lamprecht, M. R.; Clarke, C.; Kang, I. H.; Friman, O.; Guertin, D. A.; Chang, J. H.; Lindquist, R. A.; Moffat, J.; Golland, P.; Sabatini, D. M. CellProfiler: Image Analysis Software for Identifying and Quantifying Cell Phenotypes. *Genome Biology* **2006**, *7* (10), R100. https://doi.org/10.1186/gb-2006-7-10-r100.

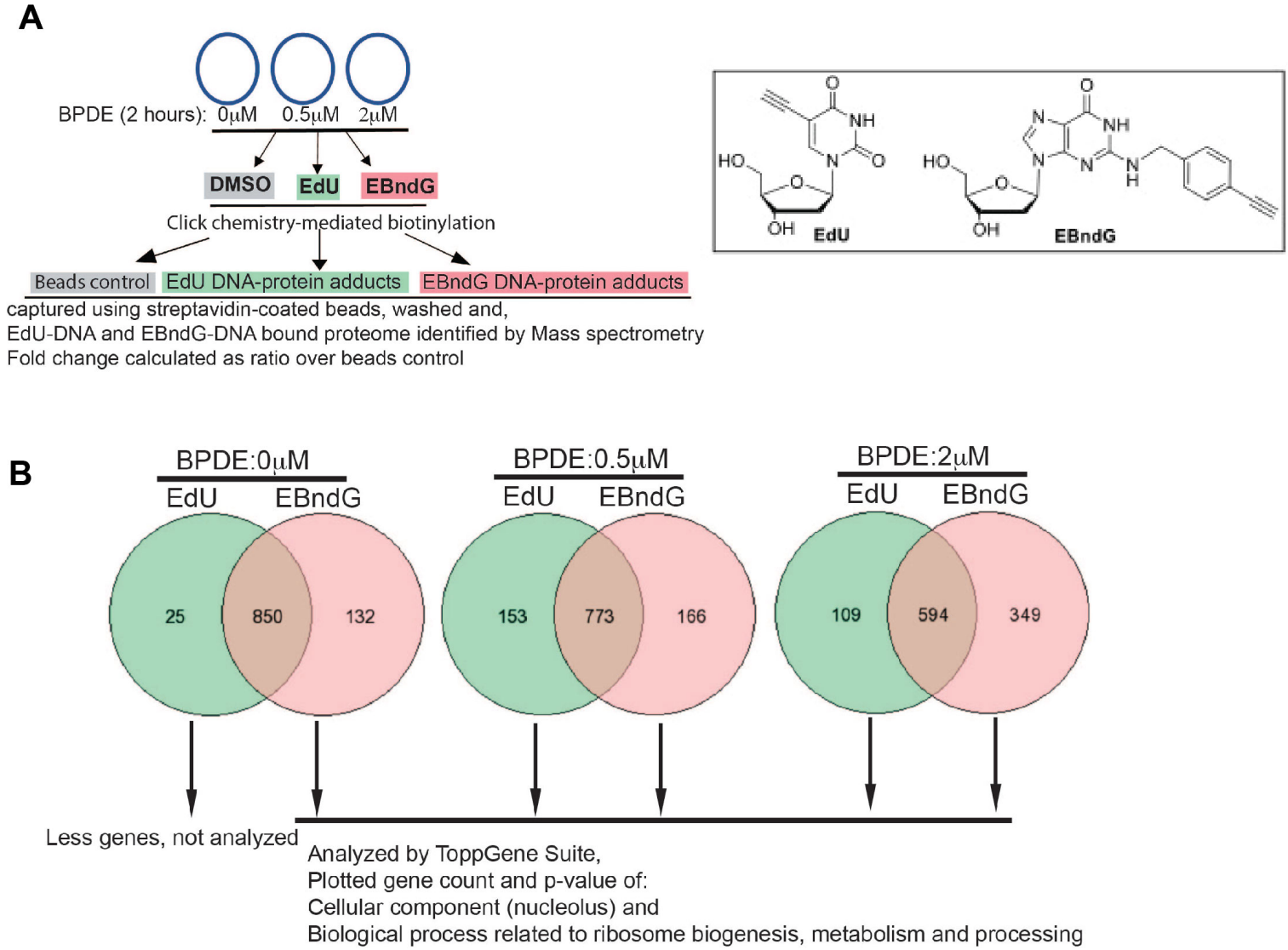

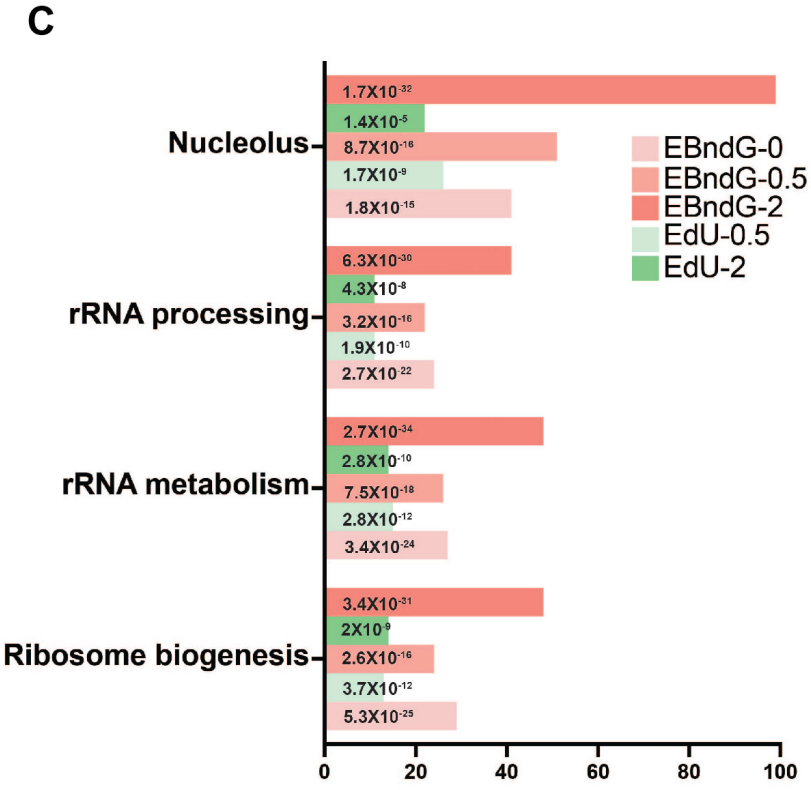

D

	GM12878			HEK293	
Symbol	0μM	0.5μM*	2μM*	2μM*	
BOP1	9.5	7.7	8	8.4	PeBoW complex
PES1	11.8	10.6	11.4	8.5	
WDR12	9.2	7.6	7.7	3.4	
NPM1	6.8	5.7	6	7	GC
UBTF	16	15.4	16.4	11	FC
FBL	13.6	12	12.4	12.8	DFC
TCOF1	2	0	1.7	6.8	
POLR1B	3	4.4	4.4	4.6	RNA Pol I
POLR1A	9.3	8.5	8.5	8.8	
PARP1	7.2	6	6.7	5.4	
RNF2	4.2	3.8	6.8	7.2	PRC
CBX8	6.3	4.3	5.6	8.6	
SUZ12	7.2	6.1	6.4	6	
EED	7.2	6	6.8	5.6	
POLK	6.9	5.4	6.7	3	

* BPDE concentration

FIGURE1

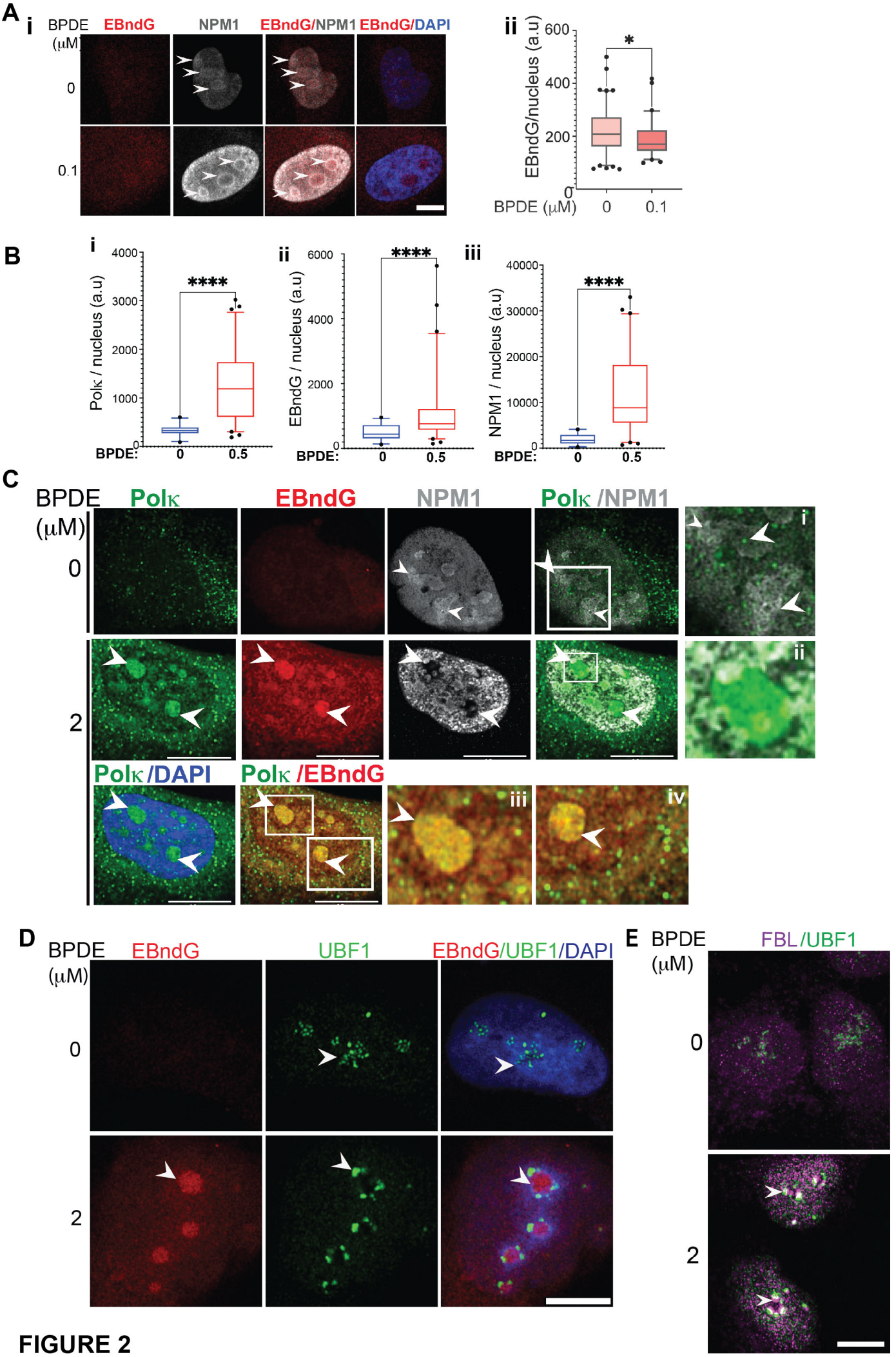
A
i
BPDE (μM)
EBndG
NPM1
EBndG/NPM1
EBndG/DAPI
0
0.1
ii
EBndG/nucleus (a.u)
600
400
200
0
*
BPDE (μM)
0
0.1
B
i
Polκ / nucleus (a.u)
4000
3000
2000
1000
0
****
BPDE:
0
0.5
ii
EBndG / nucleus (a.u)
6000
4000
2000
0
****
BPDE:
0
0.5
iii
NPM1 / nucleus (a.u)
40000
30000
20000
10000
0
****
BPDE:
0
0.5
C
BPDE (μM)
Polκ
EBndG
NPM1
Polκ /NPM1
0
2
i
ii
Polκ /DAPI
Polκ /EBndG
iii
iv
D
BPDE (μM)
EBndG
UBF1
EBndG/UBF1/DAPI
0
2
E
BPDE (μM)
FBL /UBF1
0
2

FIGURE 2

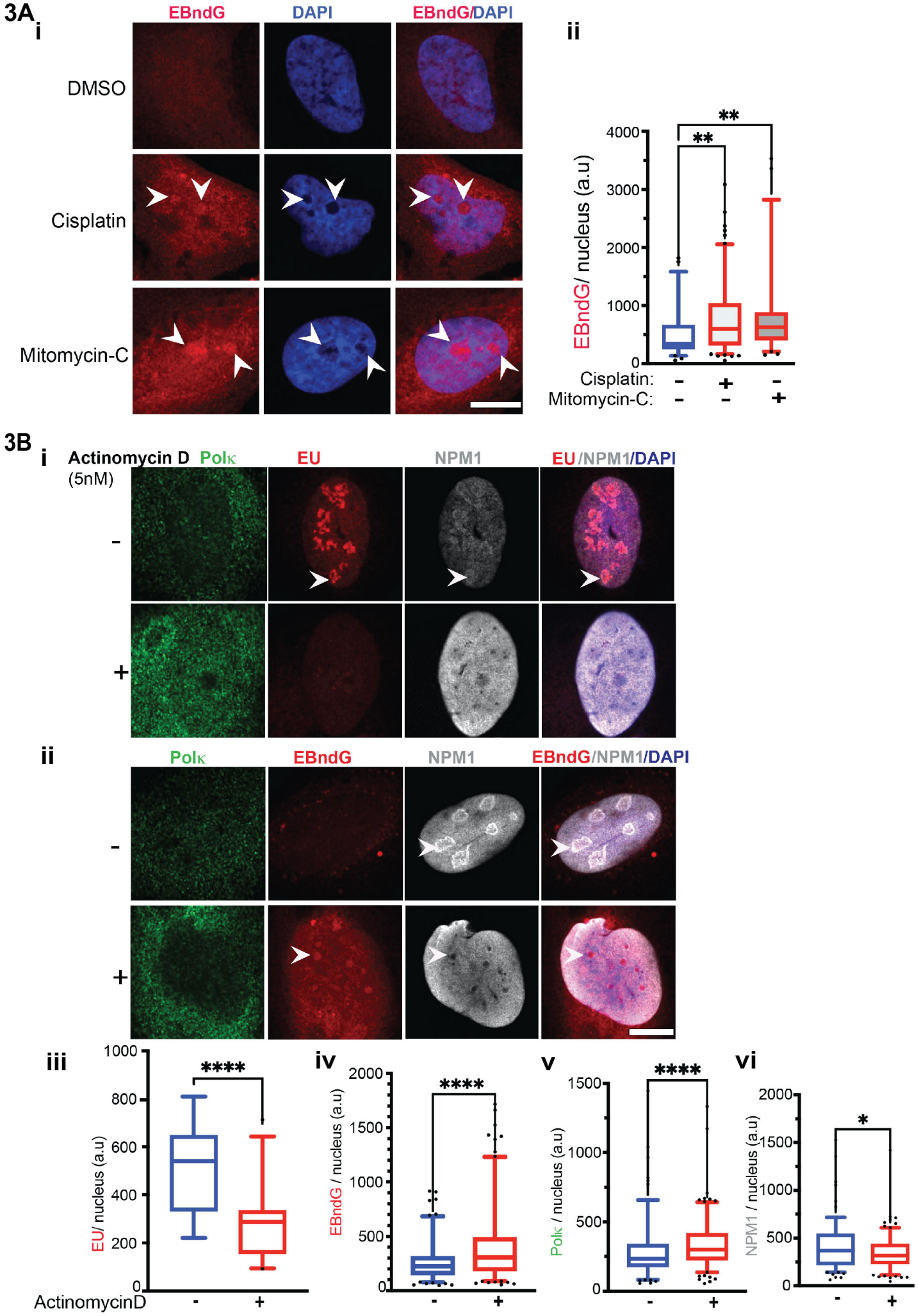
3A
i
EBndG
DAPI
EBndG/DAPI
DMSO
Cisplatin
Mitomycin-C
ii
EBndG/ nucleus (a.u)
4000
3000
2000
1000
0
**
**
Cisplatin: - + -
Mitomycin-C: - - +
3B
i
Actinomycin D (5nM)
Polκ
EU
NPM1
EU/NPM1/DAPI
-
+
ii
Polκ
EBndG
NPM1
EBndG/NPM1/DAPI
-
+
iii
EU/ nucleus (a.u)
1000
800
600
400
200
0
****
ActinomycinD - +
iv
EBndG / nucleus (a.u)
2000
1500
1000
500
0
****
- +
v
Polκ / nucleus (a.u)
1500
1000
500
0
****
- +
vi
NPM1 / nucleus (a.u)
2000
1500
1000
500
0
*
- +

FIGURE 3

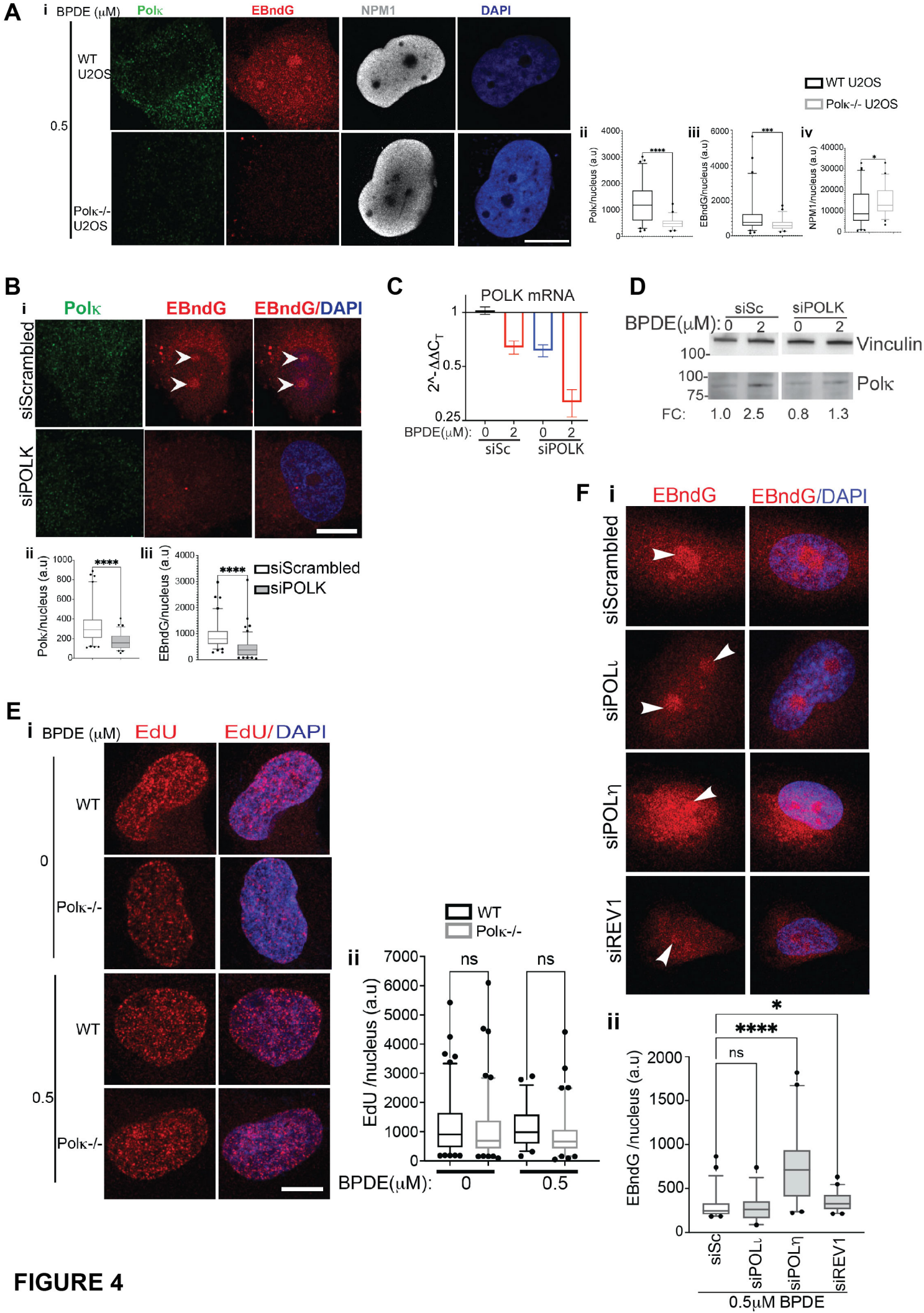
A
i BPDE (μM)
Polκ
EBndG
NPM1
DAPI
WT U2OS
0.5
Polκ-/- U2OS
WT U2OS
Polκ-/- U2OS
ii
Polκ/nucleus (a.u)
iii
EBndG/nucleus (a.u)
iv
NPM1/nucleus (a.u)
B
i
Polκ
EBndG
EBndG/DAPI
siScrambled
siPOLK
ii
Polκ/nucleus (a.u)
iii
EBndG/nucleus (a.u)
siScrambled
siPOLK
C
POLK mRNA
2^-ΔΔC_T
BPDE(μM): 0 2 0 2
siSc
siPOLK
D
siSc
siPOLK
BPDE(μM): 0 2 0 2
Vinculin
Polκ
FC: 1.0 2.5 0.8 1.3
E
i BPDE (μM)
EdU
EdU/DAPI
WT
0
Polκ-/-
WT
0.5
Polκ-/-
ii
WT
Polκ-/-
EdU /nucleus (a.u)
ns
ns
BPDE(μM): 0 0.5
F
i
EBndG
EBndG/DAPI
siScrambled
siPOLι
siPOLη
siREV1
ii
EBndG /nucleus (a.u)
siSc
siPOLι
siPOLη
siREV1
0.5μM BPDE

FIGURE 4

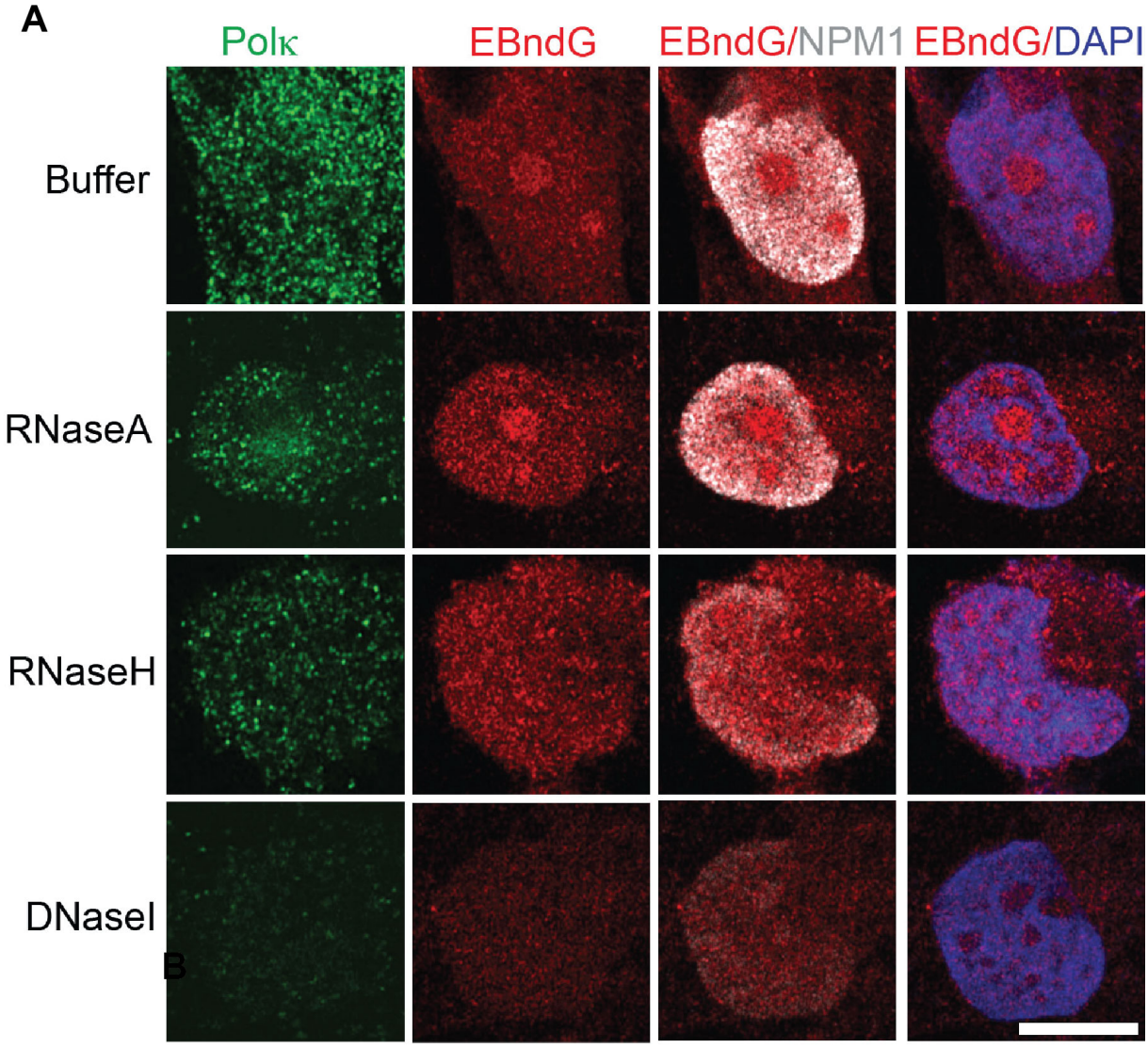
A
Polκ
EBndG
EBndG/NPM1
EBndG/DAPI
Buffer
RNaseA
RNaseH
DNaseI

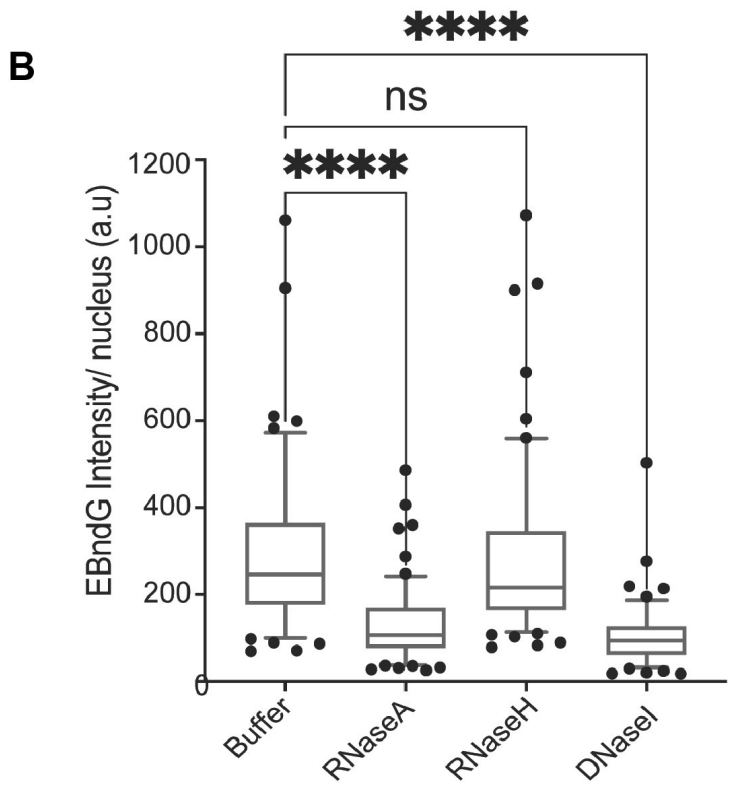
B
****
ns
****
EBndG Intensity/ nucleus (a.u)
1200
1000
800
600
400
200
0
Buffer
RNaseA
RNaseH
DNaseI

FIGURE 5

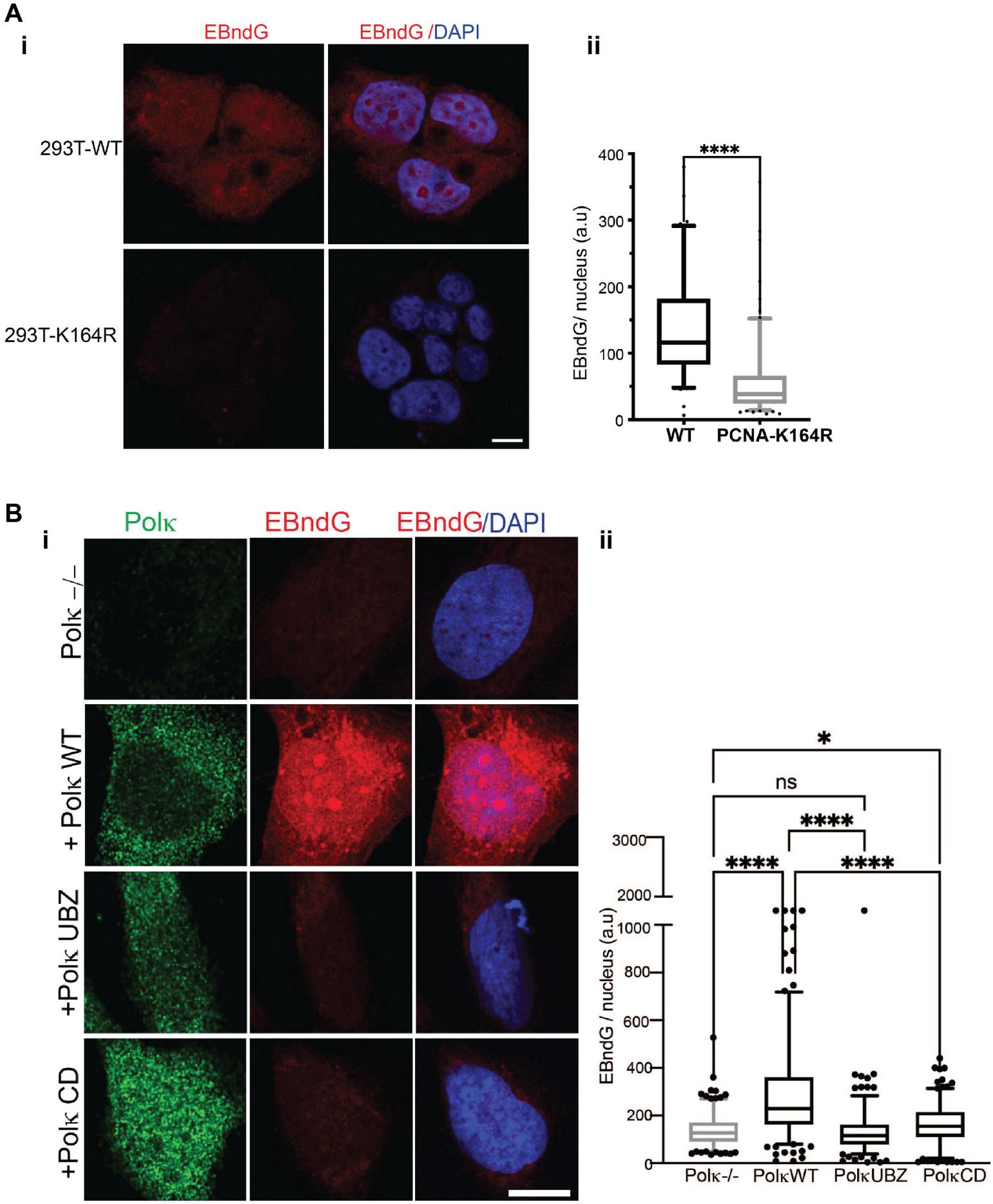
A
i
EBndG
EBndG /DAPI
293T-WT
293T-K164R
ii
****
EBndG/ nucleus (a.u)
400
300
200
100
0
WT
PCNA-K164R
B
i
Polκ
EBndG
EBndG/DAPI
Polκ −/−
+ Polκ WT
+Polκ UBZ
+Polκ CD
ii
*
ns
****
****
****
EBndG / nucleus (a.u)
3000
2000
1000
800
600
400
200
0
Polκ-/-
PolκWT
PolκUBZ
PolκCD

FIGURE 6

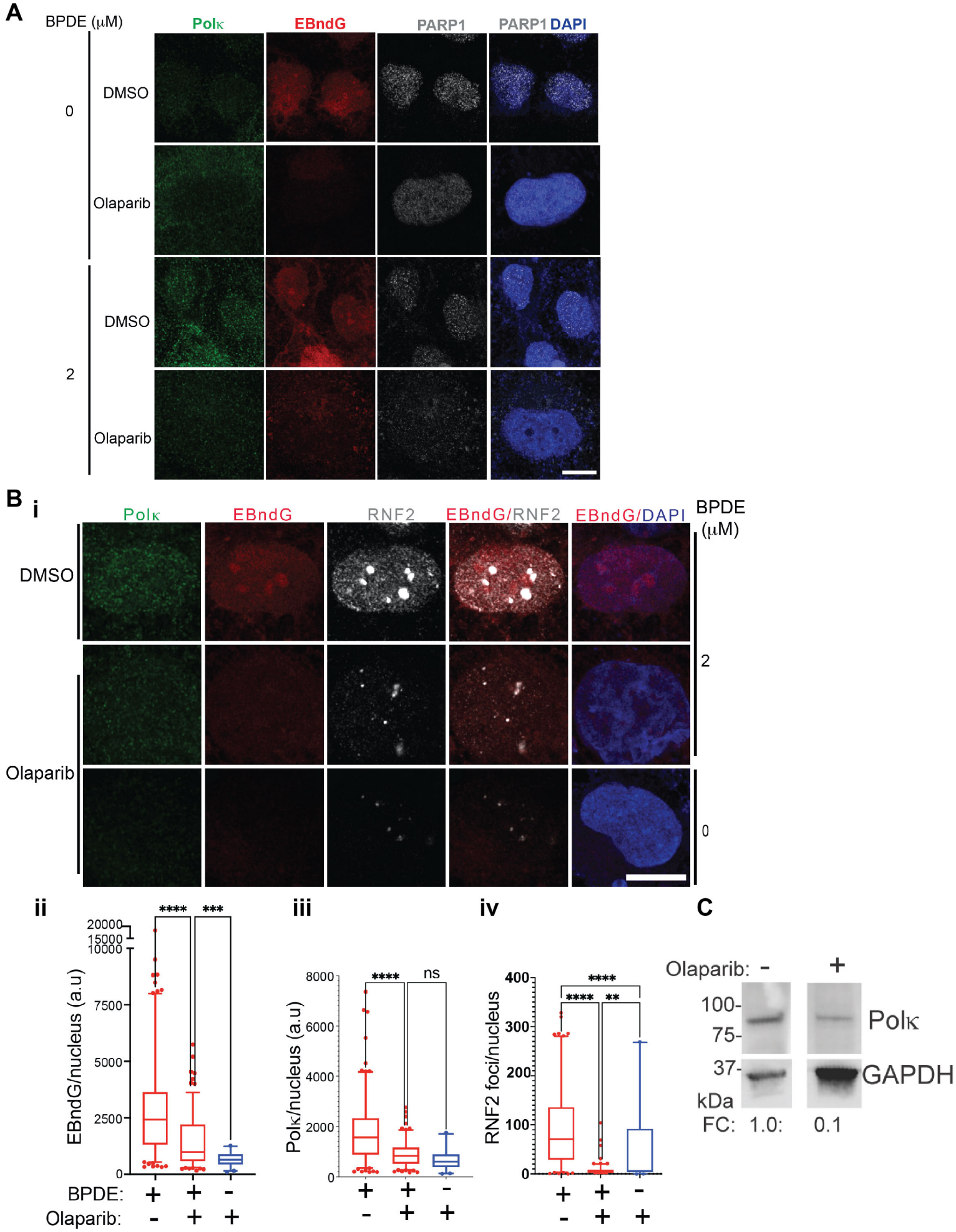
A
BPDE (μM)
Polκ
EBndG
PARP1
PARP1 DAPI
0
DMSO
Olaparib
2
DMSO
Olaparib
B
i
Polκ
EBndG
RNF2
EBndG/RNF2
EBndG/DAPI
BPDE (μM)
DMSO
Olaparib
2
0
ii
EBndG/nucleus (a.u)
BPDE:
Olaparib:
iii
Polκ/nucleus (a.u)
ns
iv
RNF2 foci/nucleus
C
Olaparib: - +
100-
75-
37-
kDa
Polκ
GAPDH
FC: 1.0: 0.1

FIGURE 7

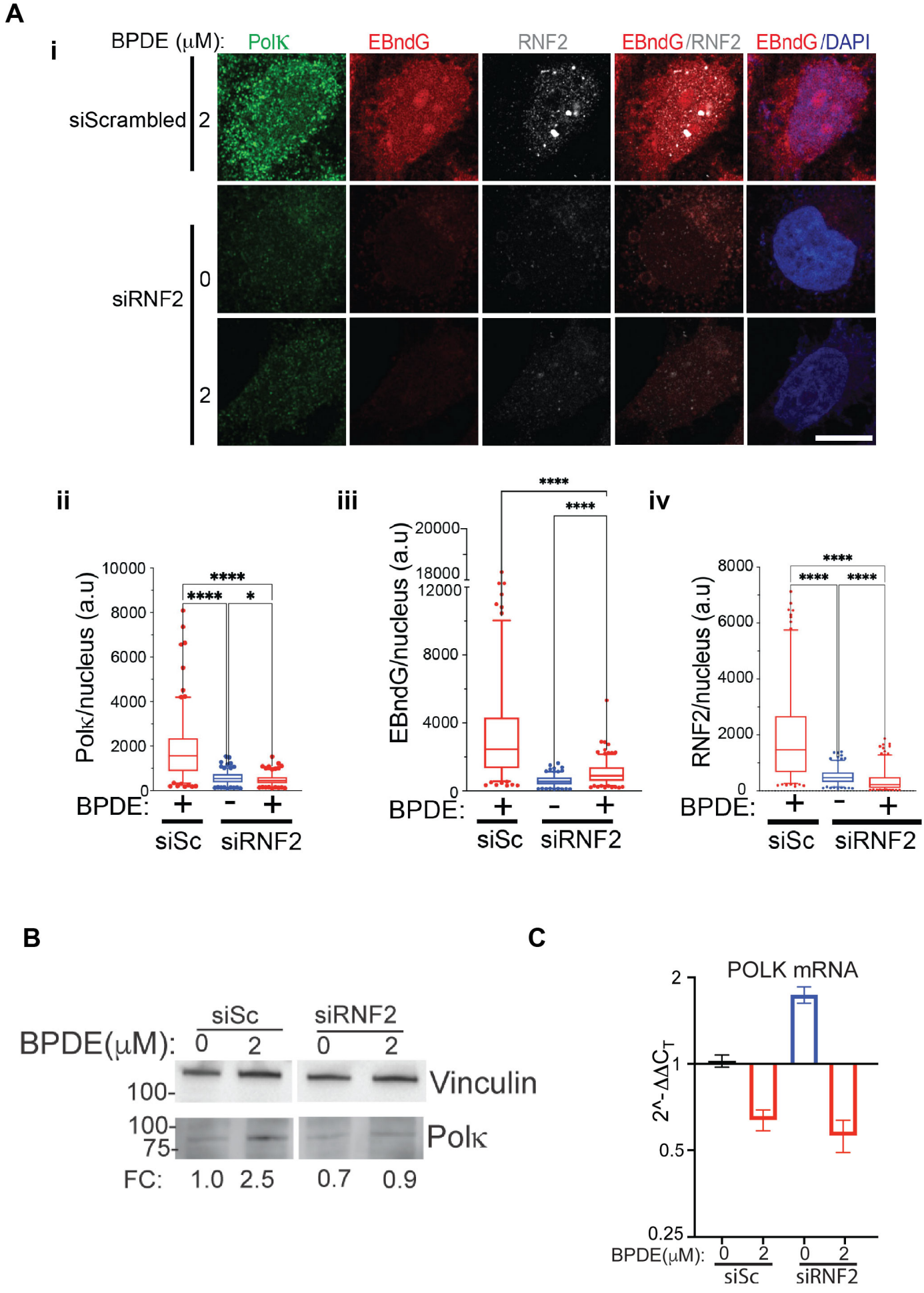
A
i
BPDE (μM):
PolK
EBndG
RNF2
EBndG/RNF2
EBndG/DAPI
siScrambled
2
siRNF2
0
2
ii
PolK/nucleus (a.u)
10000
8000
6000
4000
2000
0
****
****
*
BPDE:
+
-
+
siSc
siRNF2
iii
EBndG/nucleus (a.u)
20000
18000
12000
8000
4000
0
****
****
BPDE:
+
-
+
siSc
siRNF2
iv
RNF2/nucleus (a.u)
8000
6000
4000
2000
0
****
****
****
BPDE:
+
-
+
siSc
siRNF2
B
BPDE(μM):
siSc
siRNF2
0
2
0
2
100-
Vinculin
100-
75-
PolK
FC:
1.0
2.5
0.7
0.9
C
POLK mRNA
2^-ΔΔC_T
2
1
0.5
0.25
BPDE(μM):
0
2
0
2
siSc
siRNF2

FIGURE 8

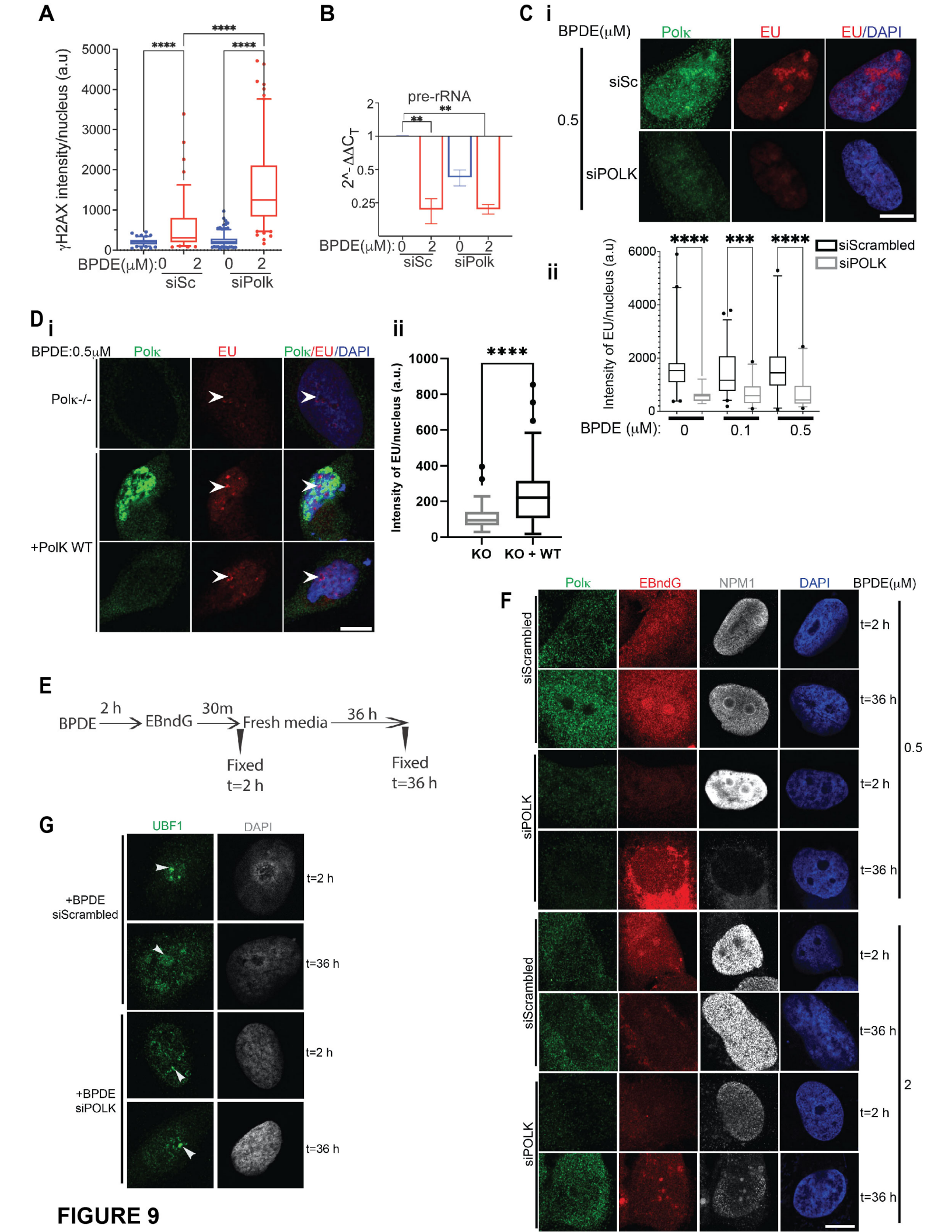
A
γH2AX intensity/nucleus (a.u)
5000
4000
3000
2000
1000
0
****
****
****
BPDE(μM):0 2 0 2
siSc
siPolk
B
pre-rRNA
2^-ΔΔC_T
2
1
0.5
0.25
**
**
BPDE(μM): 0 2 0 2
siSc
siPolk
C i
BPDE(μM)
Polκ
EU
EU/DAPI
siSc
0.5
siPOLK
ii
Intensity of EU/nucleus (a.u)
6000
4000
2000
0
****
***
****
siScrambled
siPOLK
BPDE (μM): 0 0.1 0.5
D i
BPDE:0.5μM
Polκ
EU
Polκ/EU/DAPI
Polκ-/-
+PolK WT
ii
Intensity of EU/nucleus (a.u.)
1000
800
600
400
200
0
****
KO
KO + WT
E
BPDE
2 h
EBndG
30m
Fresh media
36 h
Fixed
t=2 h
Fixed
t=36 h
F
Polκ
EBndG
NPM1
DAPI
BPDE(μM)
siScrambled
siPOLK
t=2 h
t=36 h
0.5
2
G
UBF1
DAPI
+BPDE
siScrambled
+BPDE
siPOLK
t=2 h
t=36 h

FIGURE 9

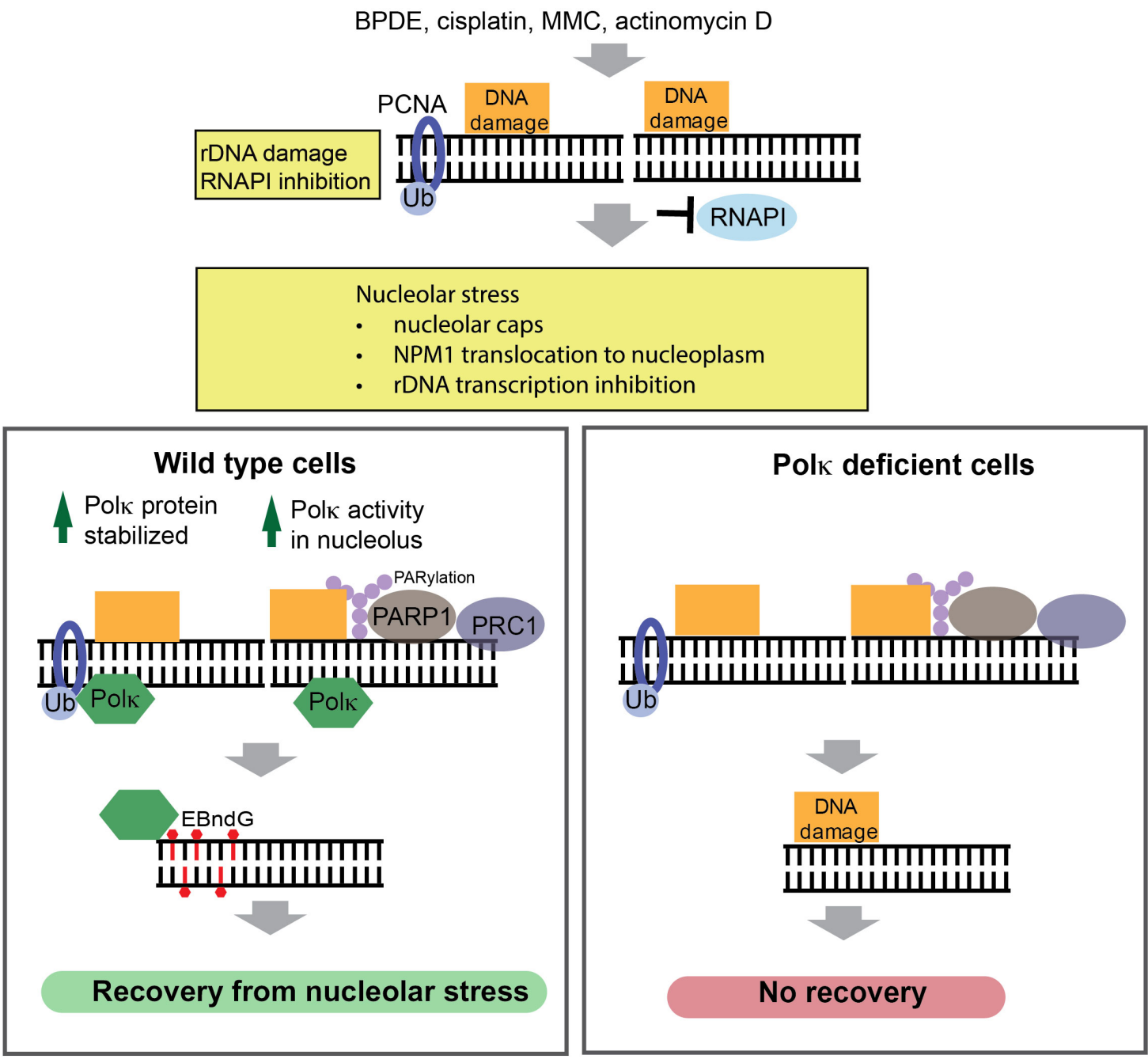
BPDE, cisplatin, MMC, actinomycin D
PCNA
DNA damage
DNA damage
rDNA damage
RNAPI inhibition
Ub
RNAPI
Nucleolar stress
• nucleolar caps
• NPM1 translocation to nucleoplasm
• rDNA transcription inhibition
Wild type cells
Polκ protein stabilized
Polκ activity in nucleolus
PARylation
PARP1
PRC1
Ub
Polκ
Polκ
EBndG
Recovery from nucleolar stress
Polκ deficient cells
Ub
DNA damage
No recovery

FIGURE 10